

Entanglement negativity in a fermionic chain with dissipative defects: Exact results

Fabio Caceffo¹ and Vincenzo Alba¹

¹Dipartimento di Fisica dell' Università di Pisa and INFN, Sezione di Pisa, I-56127 Pisa, Italy

Abstract. We investigate the dynamics of the fermionic logarithmic negativity in a free-fermion chain with a localized loss, which acts as a dissipative impurity. The chain is initially prepared in a generic Fermi sea. In the standard hydrodynamic limit of large subsystems and long times, with their ratio fixed, the negativity between two subsystems is described by a simple formula, which depends only on the effective absorption coefficient of the impurity. The negativity grows linearly at short times, then saturating to a volume-law scaling. Physically, this reflects the continuous production with time of entangling pairs of excitations at the impurity site. Interestingly, the negativity is not the same as the Rényi mutual information with Rényi index $1/2$, in contrast with the case of unitary dynamics. This reflects the interplay between dissipative and unitary processes. The negativity content of the entangling pairs is obtained in terms of an effective two-state mixed density matrix for the subsystems. Criticality in the initial Fermi sea is reflected in the presence of logarithmic corrections. The prefactor of the logarithmic scaling depends on the loss rate, suggesting a nontrivial interplay between dissipation and criticality.

1. Introduction

In recent years tremendous progress in cold-atom experiments [1, 2, 3, 4, 5, 6, 7] and the rise of Noisy-Intermediate-Scale-Quantum [8, 9] (NISQ) platforms provided us with the opportunity to test quantum mechanics with an unprecedented level of accuracy and versatility. The question how the macroscopic “classical” world emerges and interacts with the microscopic quantum one is one of the most fundamental research themes.

Here we address the question how entanglement, which is the distinctive feature of quantum mechanics, is affected by the interaction with the environment in *open* quantum many-body systems. Specifically, we consider the paradigmatic setup of a uniform Fermi sea subject to the incoherent removal of fermions at the centre of the system. This localized fermionic loss can be viewed as a dissipative impurity (see Fig. 1). We model the system-environment interaction with the Lindblad master equation [10, 11]. Recently, it has been shown that in the presence of *global* dissipation modelled by a quadratic Lindblad equation [12] it is possible to use the hydrodynamic framework to describe the dynamics of several entanglement-related quantities [13, 14, 15], such as the von Neumann entropy and Rényi entropies, the mutual information, and the logarithmic negativity [16]. These results generalize a well-established quasiparticle picture [17, 18, 19, 20, 21] for entanglement spreading to free systems with quadratic dissipation [12] *à la* Lindblad. Crucially, in the presence of an environment genuine quantum entanglement and spurious statistical correlations are deeply intertwined, since the global system is in a mixed state. Neither the von Neumann entropy nor the mutual information are proper measures of entanglement. Instead, the logarithmic negativity [22] or the fermionic logarithmic negativity [23] can be used to sieve genuine entanglement even in mixed-state systems. Moreover, while quite generically global dissipation destroys entanglement, dissipative localized impurities, such as fermionic gain/loss, can induce robust entanglement production [24].

Free systems with localized losses provide a minimal theoretical laboratory to understand the interplay between quantum and statistical correlations underpinning the entanglement growth. Statistical correlations are due to the initial homogeneous Fermi sea being progressively depleted with time. Specifically, the absorption of fermions transforms the initial zero-entropy Fermi sea in a state with finite thermodynamic entropy. This finite thermodynamic entropy is reflected in a generic growth of the von Neumann entropy [24]. At the same time, genuine entanglement production occurs. The mechanism at play is depicted in Fig. 1 (b). Each fermion in the initial state can scatter with the dissipative impurity. This leads to a continuous production in time of entangled pairs formed by the reflected and transmitted fermions. The entangled fermions propagate in the system entangling different spatial regions. A similar mechanism governs the entanglement dynamics in the presence of impurities in closed systems [25]. The production of genuine entanglement is captured by the negativity, whereas the von Neumann entropy is sensitive to both statistical and quantum correlations. Remarkably, in closed systems with defects the negativity

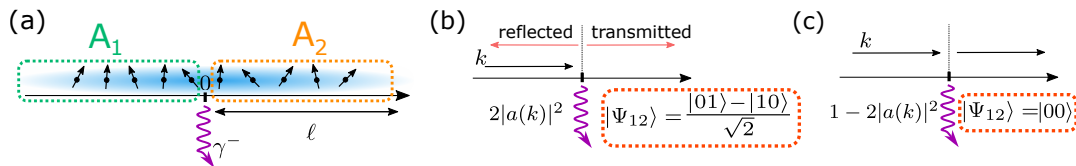


Figure 1. A free fermion chain subject to a localized fermion loss. (a) The chain is prepared in the uniform Fermi sea with Fermi momentum k_F . At the origin fermions are removed incoherently at a rate γ^- . We are interested in the fermionic logarithmic negativity between two equal intervals A_1 and A_2 of length ℓ embedded in an infinite chain and adjacent to the fermionic loss. (b) and (c) Mechanism for entanglement generation via the lossy site. In (b) a fermion with quasimomentum k is absorbed at the origin with probability $2|a(k)|^2$, with $|a(k)|^2$ the absorption coefficient. The two subsystems are put in the maximally entangled state $(|01\rangle - |10\rangle)/\sqrt{2}$, with $|0\rangle$ and $|1\rangle$ normalized states. (c) The fermion is not affected by the loss with probability $1 - 2|a(k)|^2$, implying that the two subsystems are in the product state $|00\rangle$.

becomes half of the Rényi mutual information with Rényi index $1/2$ [26, 27], similar to what found in translation invariant setups [28]. As we are going to show, this is not the case in the presence of dissipative impurities.

Specifically, here we derive a formula describing the fermionic logarithmic negativity between two equal-length intervals in a free-fermion chain in the presence of localized losses (see Fig. 1 (a)). This allows us to precisely unravel how statistical correlations trigger a linear growth of entanglement. Our formula holds in the standard hydrodynamic limit of large intervals and long times, with their ratio fixed. In this limit the negativity is described by a simple hydrodynamic formula, which depends on the absorption coefficient of the impurity [29]. The negativity grows linearly with time up to times proportional to the size of the intervals, then attaining a volume-scaling at infinite time. In contrast with the von Neumann entropy, the negativity is only sensitive to the entangled fermionic pairs produced at the impurity, as we verify by varying the geometry of the two intervals. Specifically, the negativity is proportional to the number of entangled pairs that are shared between the intervals, and it is not related to the Rényi mutual information, in contrast with the results in the unitary case [28, 26, 27]. Similar behaviour is observed for the case of global dissipation [24]. The negativity content of the quasiparticles can be derived from an effective two-state mixed density matrix for the intervals. Finally, going beyond the hydrodynamic limit, we numerically show that the negativity exhibits subleading terms that scale logarithmically with the intervals size. While these terms are reminiscent of the Fermi sea critical behaviour, their prefactor depends on the loss rate. This suggests a deep interplay between dissipation and criticality.

The outline of the paper is as follows. We start in section 2 with a review of the free-fermion chain with a localized loss. In particular, we provide the result for the fermionic correlation function (9), which is necessary to obtain the negativity. In section 3 we introduce the negativity, and its calculation in free-fermion systems. In section 4 we

present without derivation our main result (see formula (22)). We compare our results with numerical data in section 5, discussing also some interesting logarithmic corrections to the hydrodynamic limit. Finally, we conclude in section 6. In Appendix A we report the derivation of the results of section 4, in particular of formula (22). In Appendix B we discuss the tripartition of the system with A_1 and A_2 on the same side of the impurity, showing that the negativity does not grow linearly with time. Finally, in Appendix C we report the calculation of the logarithmic negativity in the low-density limit, in which there is only one fermion in the system.

2. Preliminaries: Tight-binding chain with localized losses

Here we focus on the tight-binding chain with localized losses. The Hamiltonian describes a system of free fermions hopping coherently between nearest-neighbour sites, and it is defined as

$$H = -J \sum_{x=-\infty}^{\infty} (c_x^\dagger c_{x+1} + c_{x+1}^\dagger c_x), \quad (1)$$

where c_x^\dagger and c_x are standard fermion creation and annihilation operators, and J is the hopping strength. Here we fix $J = 1$. We consider an infinite chain. The model is diagonalized by going to Fourier space, defining new fermionic operators b_k as

$$b_k := \sum_{x=-\infty}^{\infty} e^{-ikx} c_x, \quad c_x = \int_{-\pi}^{\pi} \frac{dk}{2\pi} e^{ikx} b_k. \quad (2)$$

In Fourier space Eq. (1) becomes diagonal as

$$H = \int_{-\pi}^{\pi} \frac{dk}{2\pi} \varepsilon_k b_k^\dagger b_k. \quad (3)$$

where the single-particle dispersion ε_k and the group velocity of the fermions v_k read as

$$\varepsilon_k := -2 \cos(k), \quad v_k := \frac{\partial \varepsilon_k}{\partial k} = 2 \sin(k). \quad (4)$$

The Hamiltonian (1) commutes with total number of fermions. The ground state of the chain is obtained by filling all the single-particle levels up to the Fermi momentum k_F , i.e., with $k \in [-k_F, k_F]$. Here k_F is related to the fermion density n_f as $n_f = k_F/\pi$. For $n_f = 1$ the ground state of (1) becomes a trivial band insulator. At $n_f < 1$, i.e., for $|k_F| < \pi$ the ground state is a critical state with power-law decaying correlations.

In the presence of localized losses the evolution of the system can be modelled by the Lindblad equation [10]. The evolution of the system density matrix ρ_t is described by

$$\frac{d\rho_t}{dt} = \mathcal{L}(\rho_t) = -i[H, \rho_t] + \gamma^- c_0 \rho_t c_0^\dagger - \frac{1}{2} \{ \gamma^- c_0^\dagger c_0, \rho_t \}, \quad (5)$$

where γ^- is the rate at which fermions are removed at the origin, i.e., the loss rate.

The fermionic correlation function $G_{x,y}$ is a central object to determine entanglement properties of the chain [30]. The correlation matrix is defined as

$$G_{x,y} := \text{Tr}(c_x^\dagger c_y \rho_t). \quad (6)$$

The Lindblad equation (5) can be used to obtain the dynamics of the $G_{x,y}$ as

$$\frac{dG_{x,y}}{dt} = i(G_{x+1,y} + G_{x-1,y} - G_{x,y+1} - G_{x,y-1}) - \frac{\gamma^-}{2}(\delta_{x,0} + \delta_{y,0})G_{x,y}. \quad (7)$$

Eq. (7) is obtained by observing that the dynamics of a generic observable \hat{O} from (5) is obtained as

$$\frac{d\hat{O}}{dt} = \mathcal{L}^\dagger(\hat{O}), \quad (8)$$

where the Liouvillian operator \mathcal{L} is defined in (5). Eq. (7) is obtained by choosing $\hat{O} = c_x^\dagger c_y$, by taking the expectation value $\langle \cdot \rangle = \text{Tr}(\cdot \rho)$, and using Wick theorem.

If the initial state is a Fermi sea with Fermi momentum k_F , Eq. (7) can be solved by using a product ansatz for $G_{x,y}$ as

$$G_{x,y}(t) = \int_{-k_F}^{k_F} \frac{dk}{2\pi} S_{k,x} \bar{S}_{k,y}, \quad (9)$$

with $S_{k,x}$ to be determined, and the bar in $\bar{S}_{k,x}$ denoting complex conjugation. For generic x, t the final result is cumbersome, although it can be obtained in some cases (see, for instance, Ref. [31] for the case with $k_F = \pi$). However, in the hydrodynamic limit $x, y, t \rightarrow \infty$ with $x/t, y/t$ fixed and $|x - y|/t \rightarrow 0$, $S_{k,x}$ takes the simple form as [29]

$$S_{k,x} = e^{ikx} + \Theta(|v_k|t - |x|)r(k)e^{i|kx|}. \quad (10)$$

Eq. (10) suggests that in the hydrodynamic limit the dissipative site acts like an impurity. In (10), v_k is the fermion group velocity (4), $\Theta(z)$ the Heaviside step function, and $r(k)$ is the reflection amplitude. Here reflection and transmission amplitudes $r(k), t(k)$ are defined as [29]

$$r(k) := -\frac{\gamma^-}{2} \frac{1}{\frac{\gamma^-}{2} + |v_k|}, \quad t(k) := \frac{|v_k|}{\frac{\gamma^-}{2} + |v_k|}. \quad (11)$$

A similar expression as Eq. (10) is obtained considering the one-dimensional scattering problem of a plane wave on a delta potential with imaginary strength [32], i.e., $V(x) = -i\gamma/2\delta(x)$. Now, the solution of the Schrödinger equation has the form $e^{ikx} + r'(k)e^{-ikx}$, with

$$r'(k) = -\frac{\gamma}{2} \frac{1}{\frac{\gamma}{2} + \frac{\hbar^2 k}{m}}. \quad (12)$$

Clearly, $r'(k)$ becomes the same as $r(k)$ in (11) after redefining $\hbar^2 k/m \rightarrow |v_k|$.

Since the dynamics is not unitary, one has that $|r(k)|^2 + |t(k)|^2 \neq 1$. One can define the absorption coefficient for the fermions $a(k)$ as

$$|a(k)|^2 := 1 - |r|^2 - |t|^2 = \gamma^- \frac{|v_k|}{\left(\frac{\gamma^-}{2} + |v_k|\right)^2}. \quad (13)$$

Eq. (10) can be rewritten as

$$S_{k,x} = e^{ikx} + r(k)e^{i|kx|} \int_{-\infty}^{\infty} \frac{dq}{2\pi i} \frac{e^{i(|v_k|t - |x|)q}}{q - i0^+}, \quad (14)$$

where the integral in the second term is used to represent the Heaviside step in (10), and $i0^+$ is an infinitesimal shift along the positive imaginary axis.

3. Entanglement negativity for fermionic systems: Definitions

We are interested to quantify the entanglement between two adjacent regions A_1 and A_2 of equal length ℓ adjacent to the dissipative impurity (see Fig. 1 (a)). Due to the presence of dissipation, the chain is not in a global pure state. This implies that neither the Rényi entropies (and von Neumann entropy) nor the mutual information are proper entanglement measures of the entanglement between A_1 and A_2 . In this situation, only the logarithmic negativity provides a proper entanglement measure. Here we consider the *fermionic* logarithmic negativity [23]. In contrast with the standard definition of negativity [22], the fermionic one can be effectively computed from the fermionic two-point correlation function (cf. (6)). To introduce the negativity, one first defines the restricted correlation matrix G_A as

$$G_A := G_{x,y}, \quad \text{with } x, y \in A, \quad (15)$$

where $G_{x,y}$ is given in (6), and the matrix Γ_A as

$$\Gamma_A := \mathbb{1} - 2G_A. \quad (16)$$

To proceed, one defines the two matrices Γ_A^\pm as

$$\Gamma_A^\pm = \begin{pmatrix} -\Gamma_A^{11} & \pm i\Gamma_A^{12} \\ \pm i\Gamma_A^{21} & \Gamma_A^{22} \end{pmatrix}, \quad \Gamma_A^{ij} := \Gamma_{x,y} \text{ with } x \in A_i, y \in A_j. \quad (17)$$

The fermionic logarithmic negativity is defined as [33, 34, 23, 35].

$$\mathcal{E} := \text{Tr} \ln \left[\sqrt{\frac{\mathbb{1} - \Xi_A}{2}} + \sqrt{\frac{\mathbb{1} + \Xi_A}{2}} \right] + \text{Tr} \ln \left[\sqrt{G_A^2 + (\mathbb{1} - G_A)^2} \right], \quad (18)$$

where Ξ_A is defined as

$$\Xi_A := P^{-1}(\Gamma_A^+ + \Gamma_A^-), \quad P := \mathbb{1} + \Gamma_A^+ \Gamma_A^-. \quad (19)$$

In (19), Γ_A^\pm are defined in (17), and $\mathbb{1}$ is the $2\ell \times 2\ell$ identity matrix.

For the following it is useful to compare the fermionic negativity with the original negativity [22]. The logarithmic negativity is defined in terms of the so-called partially transposed reduced density matrix. Given the reduced density matrix ρ_A for $A_1 \cup A_2$ (see Fig. 1), we define the partial transpose $\rho_A^{\text{T}_2}$ as

$$\langle e_i^{(1)} \otimes e_j^{(2)} | \rho_A^{\text{T}_2} | e_k^{(1)} \otimes e_l^{(2)} \rangle := \langle e_i^{(1)} \otimes e_l^{(2)} | \rho_A | e_k^{(1)} \otimes e_j^{(2)} \rangle, \quad (20)$$

where we denoted with $e_j^{(1)}$ and $e_j^{(2)}$ two bases for the Hilbert space of A_1 and A_2 , respectively. For non-separable states, the partial transpose is not, in general, a positive-definite matrix, in contrast with ρ_A . The negative eigenvalues of $\rho_A^{\text{T}_2}$ quantify the entanglement shared between the two intervals. The logarithmic negativity is defined as

$$\mathcal{E} := \ln(\text{Tr}|\rho_A^{\text{T}_2}|). \quad (21)$$

Unfortunately, calculating the logarithmic negativity [36, 22, 37, 38, 39] in quantum-many-body systems is in general a challenging task [40, 41], except for free-boson systems [42]. For free fermions the partial transpose cannot be written as a Gaussian fermionic operator, implying that its spectrum, and hence the negativity, cannot be computed effectively [40].

Extracting the salient physical information, such as the scaling behaviour, of the negativity is in general challenging task. Still, several results are available. For equilibrium systems described by Conformal Field Theory, the scaling of the ground-state logarithmic negativity is known analytically [39, 43, 34], also at finite-temperature [43, 35]. The behaviour of the negativity in massive quantum field theory was also investigated [44, 45]. For CFT systems, scaling properties of the full spectrum of the partial transpose are known [46, 47]. Interestingly, both the standard and the fermionic logarithmic negativity exhibit logarithmic scaling in random singlet phases of matter [48, 34]. The behaviour of the logarithmic negativity at finite-temperature criticality in quantum models has been investigated [49, 50, 51]. Interestingly, the dynamics of negativity in integrable systems after a quantum quench [52] can be described within the quasiparticle picture [53]. In the hydrodynamic regime of validity of the quasiparticle picture, both the fermionic and the standard negativity become half of the Rényi mutual information [28] with Rényi index $1/2$. This surprising result has been verified in free-fermion and free-boson models [28], in free-fermion chains in the presence of defects [26], and in Conformal Field Theory [54, 55, 56]. A rigorous derivation is also possible in minimal models of interacting quantum many-body systems, such as dual unitary circuits [57, 58]. Besides the negativity, the moments of the partial transpose, or the $PPT - n$ conditions, can be employed to quantify entanglement in many-body systems. The $PPT - n$ conditions can be also measured experimentally [4], and admit a quasiparticle picture interpretation [?]. Some results are also available for disordered out-of-equilibrium systems [60].

In the context of dissipative quantum many-body systems, the scaling of the fermionic logarithmic negativity has been investigated in the weakly-dissipative limit for free-fermions with gain and loss dissipation [16]. While a hydrodynamic description of the negativity is possible, the negativity content of the quasiparticles has no straightforward interpretation in terms of thermodynamic quantities. In particular, the relationship between negativity and mutual information established in Ref. [28] is violated. Very recently, the negativity has been studied in the context of free-fermions undergoing continuous monitoring [61, 62].

4. Logarithmic negativity in the presence of localized losses: Main result

Here we outline our main result. Let us consider the setup depicted in Fig. 1: Two equal-length intervals A_1 and A_2 are placed next to the dissipative impurity in an infinite chain. In the hydrodynamic limit $t, \ell \rightarrow \infty$ with the ratio t/ℓ fixed, and for generic loss rate γ^- ,

the fermionic logarithmic negativity between A_1 and A_2 is given as

$$\mathcal{E} = \frac{\ell}{2} \int_{-k_F}^{k_F} \frac{dk}{2\pi} \min(|v_k|t/\ell, 1) e(1 - 2|a(k)|^2) \quad (22)$$

with v_k the fermion velocity (4), and $e(x)$ defined as

$$e(x) := \ln \left(1 - x + \sqrt{x^2 + (1 - x)^2} \right). \quad (23)$$

The negativity (22) depends only on the absorption coefficient $|a(k)|^2$ of the impurity (cf. (13)). From Eq. (22) one has that \mathcal{E} grows linearly with time for $t < \ell/v_{\max}$, where v_{\max} (cf. (4)) is the maximum velocity for the fermions. Notice that v_{\max} depends on the initial state via k_F . At asymptotically long times, \mathcal{E} saturates, and it exhibits a volume-law scaling $\mathcal{E} \sim \ell$. The physical interpretation of the growth of the negativity is as follows. As anticipated, the localized loss acts as a dissipative impurity. The fermions in the initial state scatter on the impurity giving rise to a superposition between transmitted and reflected fermions, which form entangled pairs (see Fig. 1 (b)). The propagation of these entangled pairs in the bulk of the system gives rise to the entanglement between the two intervals. Specifically, if the reflected fermion is in A_1 and the transmitted is in A_2 they contribute to the negativity between them. The min function in (22) counts the number of entangled pairs there are shared between the two subsystems. Finally, as there is a finite density of fermions in the initial state, there is a continuous production in time of entangled pairs, which sustain the linear growth of \mathcal{E} . A similar mechanism explains the behaviour of the entanglement entropy and of the negativity in free-fermion systems undergoing unitary dynamics in the presence of defects [25, 63, 26, 64, 65, 27, 66]. More generically, the propagation of entangled pairs of quasiparticle excitations is the underlying mechanism for the entanglement dynamics in integrable systems [17, 18, 19, 67] (see, however, Ref. [68] and Ref. [69] for recent developments), also in the presence of quadratic Lindblad dissipation [13, 14]. The derivation of (22) is technically involved, although the main tool is the multi-dimensional stationary phase approximation [70], together with the results of Ref. [24]. We report the derivation of (22) in Appendix A.

Instead, we now discuss the physical interpretation of the negativity content $e(k)$ (cf. (23)) of the entangled pairs. Crucially, $e(k)$ is understood in terms of a two-level system for the subsystems. Let us introduce a fictitious state $|s_1 s_2\rangle$ for $A_1 \cup A_2$. Here s_i can take the values 0, 1. We can write the following density matrix for $A_1 \cup A_2$ as

$$\rho_{A_1 \cup A_2} = (1 - 2|a(k)|^2)|00\rangle\langle 00| + |a(k)|^2 (|01\rangle - |10\rangle)(\langle 01| - \langle 10|). \quad (24)$$

The interpretation of (24) is that at the beginning the system is in the unperturbed product state $|00\rangle$ and the subsystems are not entangled with each other. The presence of the dissipation, then, drives the system in the antisymmetric maximally entangled state $(|01\rangle - |10\rangle)/\sqrt{2}$ with probability $2|a(k)|^2$. The effective density matrix (24) and the mechanism by which fermion absorption leads to entanglement production can be

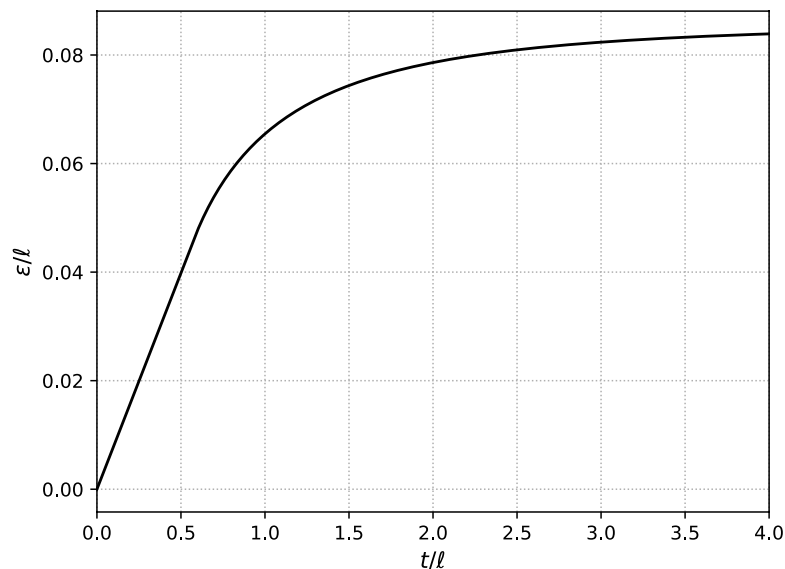


Figure 2. Typical behavior of the fermionic negativity \mathcal{E} in the free-fermion chain with localized losses. The curve is the analytic result (cf. (22)) for a chain prepared in a Fermi sea with $k_F = \pi/3$ and loss rate $\gamma^- = 1$. In the figure we show \mathcal{E}/ℓ versus t/ℓ , with ℓ the size of the two subsystems (see Fig. 1). Notice the linear increase up to $t/\ell = v_{\max}$, followed by a saturating behavior for $t/\ell \rightarrow \infty$.

also understood by considering the low-density limit in which there is only one fermion in the chain (see Appendix C). The partially transposed reduced density matrix with respect to A_2 is obtained from (24) as

$$\rho_{A_1 \cup A_2}^{T_2} = (1 - 2|a(k)|^2)|00\rangle\langle 00| + |a(k)|^2 (|10\rangle\langle 10| + |01\rangle\langle 01| - |00\rangle\langle 11| - |11\rangle\langle 00|). \quad (25)$$

By calculating the negativity (21) from (25) one obtains (23) with $x = 1 - 2|a(k)|^2$. Notice that here we are considering the original negativity (21), and not the fermionic one (18). Interestingly, the fact that from (25) we recover the $e(k)$ for the fermionic negativity could suggest that in the hydrodynamic limit the two definitions of the negativity are equivalent. This happens, for instance, if the dynamics is unitary [28]. However, checking this prediction is challenging because of the serious limitations of analytical and numerical methods to compute the negativity (21) in out-of-equilibrium fermionic systems. As it is clear from (22), the equality between Rényi mutual information and negativity established in [28] does not hold in the presence of dissipative impurities, although the fermionic negativity and the original one could become the same in the hydrodynamic limit. We should also mention that the functional form of $e(k)$ is reminiscent of the negativity between two intervals in a chain with a single fermion (see Appendix C for the result). Eq. (22) holds only for two adjacent intervals (see Fig. 1), although it can be straightforwardly generalized to different geometries. Indeed, the function $e(k)$ remains the same, whereas the function $\min(|v(k)t|/\ell, t)$ has to be modified to account for the different kinematics of the quasiparticles. Importantly, for the geometry with the two intervals next to the impurity as in Fig. 1, both the

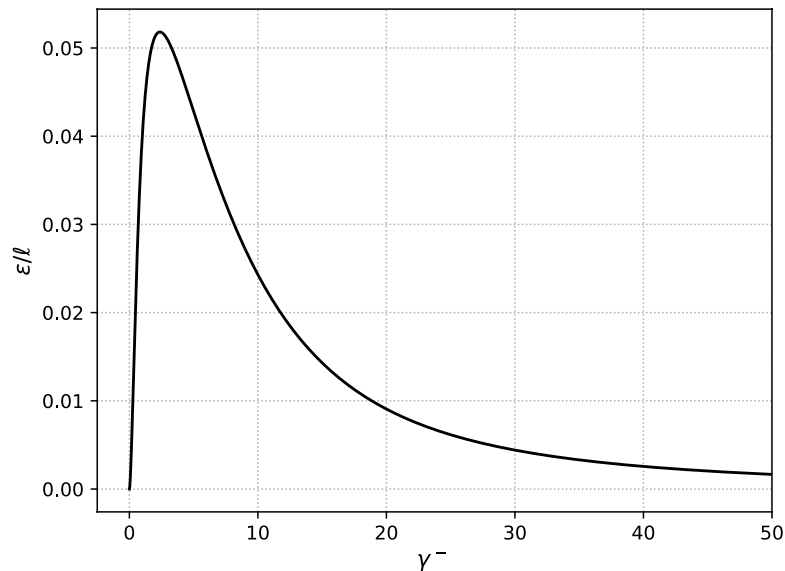


Figure 3. Logarithmic negativity \mathcal{E}/ℓ as a function of the loss rate γ^- at fixed $t/\ell = 0.5$ and $k_F = \pi/3$. The figure shows the analytic result in the hydrodynamic limit $t, \ell \rightarrow \infty$ with t/ℓ fixed (cf. (22)). Note the vanishing behavior for $\gamma^- \rightarrow \infty$.

negativity and the von Neumann entropy grow with time [24]. On the other hand, while the von Neumann entropy is sensitive to both statistical correlations and entanglement, the negativity is sensitive to entanglement only. This can be verified by considering the geometry with both intervals on the same side of the impurity. This is discussed in Appendix B. Since the reflected and transmitted fermions are created at the impurity site and travel in opposite directions, they cannot be shared between the two intervals, implying that no entanglement is produced. While in this situation the von Neumann entropy is still nonzero [24], i.e., it fails to distinguish between classical and quantum correlations, the negativity vanishes in the scaling limit, as we prove in Appendix B.

The generic behaviour of (22) as a function of time is illustrated in Fig. 2. In the figure we show results for $k_F = \pi/3$. The setup is the same as in Fig. 1 (a). To highlight the scaling behaviour we plot \mathcal{E}/ℓ versus t/ℓ . As discussed above, \mathcal{E}/ℓ grows linearly with time up to $t^* = 1/v_{\max}$. Here $v_{\max} = v_{\pi/3} < 1$ (cf. (4)). For $t \gg t^*$ the negativity saturates at asymptotically long times. It is interesting to investigate the behaviour of the negativity as a function of the loss rate γ^- . This is discussed in Fig. 3. We plot \mathcal{E}/ℓ versus γ^- at fixed $t/\ell = 1/2$. The negativity exhibits a maximum at intermediate times, then it decreases, vanishing in the limit $\gamma^- \rightarrow \infty$. A similar behaviour is observed for the von Neumann entropy [24]. The vanishing behaviour at $\gamma^- \rightarrow \infty$ is a manifestation of the quantum Zeno effect [71, 72, 73]. Precisely, in the limit $\gamma^- \rightarrow \infty$ the absorption and the transmission coefficients vanish (cf. (11) and (13)), whereas the reflection coefficient $|r(k)|^2$ goes to one. This means that at large γ^- the two halves of the chain are effectively decoupled.

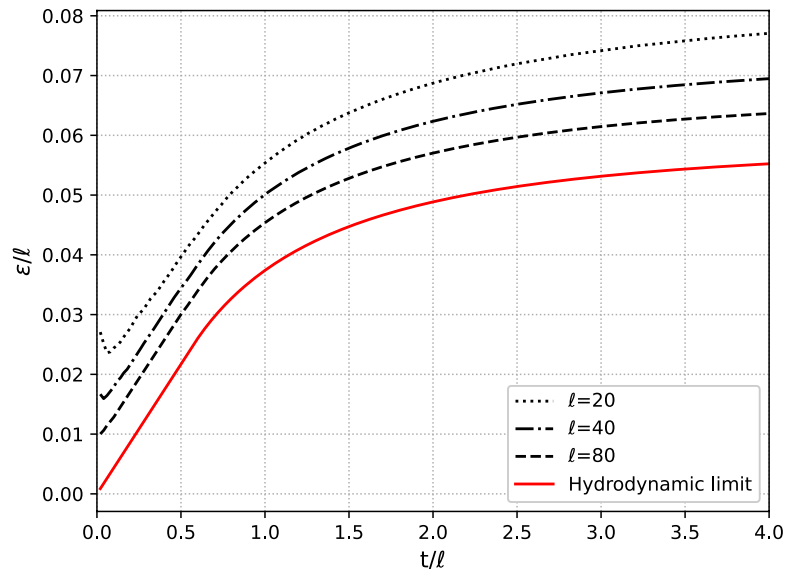


Figure 4. Logarithmic negativity between two equal intervals in a free-fermion chain with a localized loss. Comparison between the theoretical prediction (22) in the hydrodynamic limit (red continuous line) and numerical results for finite interval size ℓ up to $\ell = 80$. Data are for fixed loss rate $\gamma^- = 0.5$. The chain is initially prepared in a Fermi sea with $k_F = \pi/3$. Upon increasing ℓ the data approach the result in the hydrodynamic limit.

5. Numerical checks & logarithmic corrections

We now discuss numerical benchmarks of our main formula (22), comparing it against exact numerical data. The data are obtained by solving numerically (7). The obtained fermionic correlator $G_{x,y}$ is then used to compute the negativity (see section 3). Eq. (7) is solved for a finite chain of length L , with open boundary conditions. In our simulations we ensure that $t \ll L$ to avoid revival effects due to open boundary conditions.

In Fig. 4 we show data for \mathcal{E}/ℓ plotted versus t/ℓ for the system with $\gamma^- = 0.5$ and $k_F = \pi/3$. We show the theory prediction (22) (continuous line) and exact numerical results for subsystem sizes $\ell = 20, 40, 80$. Clearly, the finite-size data exhibit noticeable deviations from the hydrodynamic limit. Still, upon increasing ℓ the data approach (22). To confirm that, in Fig. 5 we restrict ourselves to the region $t/\ell \leq 1$ showing data up to $\ell = 640$. As it is clear from the figure, the slope of the data with the largest $\ell = 640$ is compatible with (22).

However, we should mention that corrections seem to decay in a slower manner as compared with the case of global dissipation [16]. To understand the origin of this fact, we now investigate the subleading terms in (22). First, since the initial state is a Fermi sea, at $t = 0$ the negativity exhibits logarithmic scaling [39] with the size ℓ . It is natural to conjecture that similar logarithmic scaling survives in the presence of loss. This suggests that

$$\mathcal{E} = \mathcal{E}_{\text{asy}} + \alpha(k_F, \gamma^-) \ln(\ell) + \mathcal{O}(1), \quad (26)$$

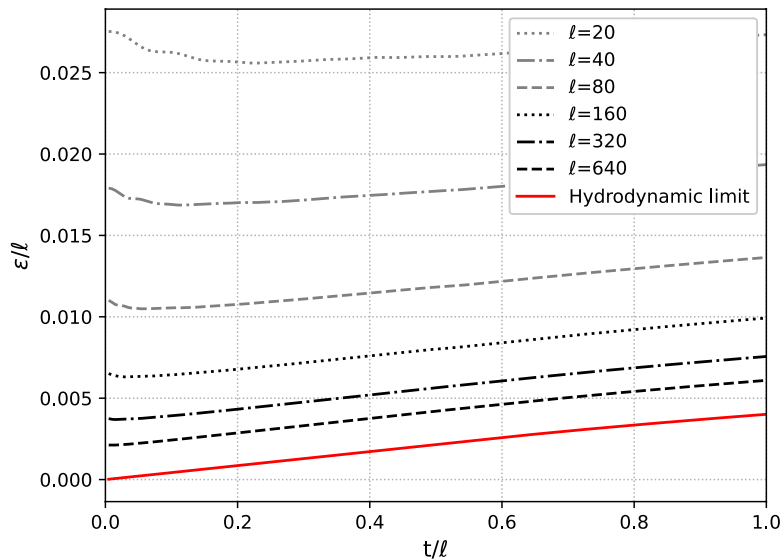


Figure 5. Same as in Fig. 4 for $t/\ell \leq 1$ and larger subsystem sizes ℓ up to $\ell = 640$.

where \mathcal{E}_{asy} is given by (22), and $\alpha(k_F, \gamma^-)$ is a constant, which in principle depends on γ^- and k_F . Now, for $\gamma^- \rightarrow 0$, the linear growth is absent, i.e., $\mathcal{E}_{\text{asy}} \rightarrow 0$, and [39]

$$\alpha(k_F, 0) \rightarrow \frac{c}{4}, \quad (27)$$

where $c = 1$ is the central charge of the Conformal Field Theory [74] (CFT) describing the long-wavelength properties of the Fermi sea. Notice that (27) does not depend on k_F . Similar logarithmic corrections as in (26) should be expected for the von Neumann entropy [24].

To check the validity of (26) we fix $t/\ell = 0.5$ plotting the difference $\mathcal{E} - \mathcal{E}_{\text{asy}}$ versus ℓ . This is reported in Fig. 6 for several values of k_F and γ^- . Clearly, $\mathcal{E} - \mathcal{E}_{\text{asy}}$ exhibits a mild increase upon increasing ℓ . The continuous lines are fits to the logarithmic increase $\mathcal{E} - \mathcal{E}_{\text{asy}} = c \ln(\ell) + d$, with c, d fitting parameters. The quality of the fits is satisfactory already for $\ell \gtrsim 200$, supporting the conjectured expression (26). Typical fitted values for c, d are $c \simeq 0.2, d \simeq -0.1$ for $\gamma^- = 0.5, k_F = \pi/3$. Interestingly, α exhibits a nontrivial dependence on γ^- . This is better illustrated in Fig. 7 plotting the same data using a logarithmic scale on the x -axis. The different slopes that we observe for the data with fixed $k_F = \pi/3$ and $\gamma^- = 0.5, \gamma^- = 0.1$ suggest that α depends on γ^- . Notice also that the comparison between the data with $k_F = \pi/3$ and $k_F = \pi/6$ at fixed $\gamma^- = 0.5$ suggests that α depends on k_F , although this could be a finite-size effect. Finally, one should remark that similar subleading logarithmic terms have been observed in the scaling of the von Neumann entropy in the presence of defects [27].

6. Conclusion

We investigated genuine entanglement propagation in a one-dimensional Fermi sea subject to both unitary and dissipative dynamics due to the presence of a localized

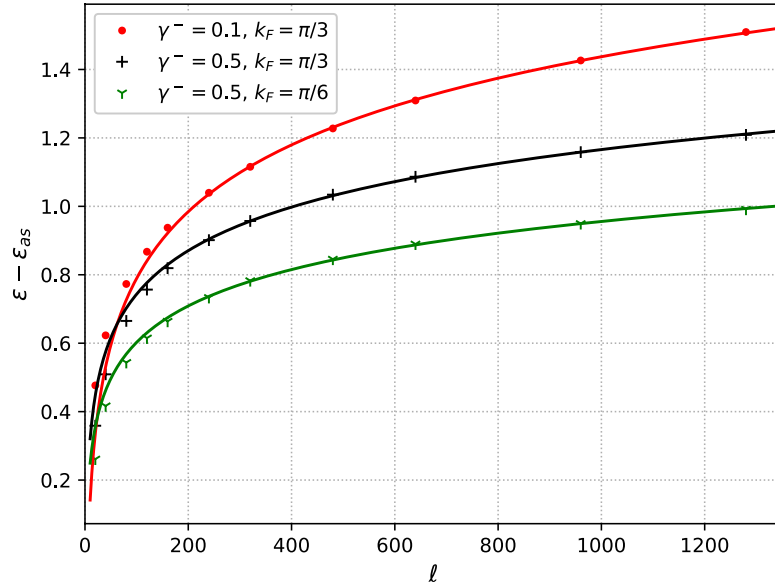


Figure 6. Logarithmic negativity \mathcal{E} in a free fermion chain with localized loss: Deviations from the hydrodynamic limit. We plot $\mathcal{E} - \mathcal{E}_{as}$, with \mathcal{E}_{as} the analytic result in the hydrodynamic limit (cf. (22)), versus ℓ . Data are for fixed $t/\ell = 0.5$. The symbols are data for different loss rate γ^- and Fermi momentum k_F . The continuous lines are fits to $\mathcal{E} - \mathcal{E}_{as} = c \ln(\ell) + d$, with c, d fitting parameters.

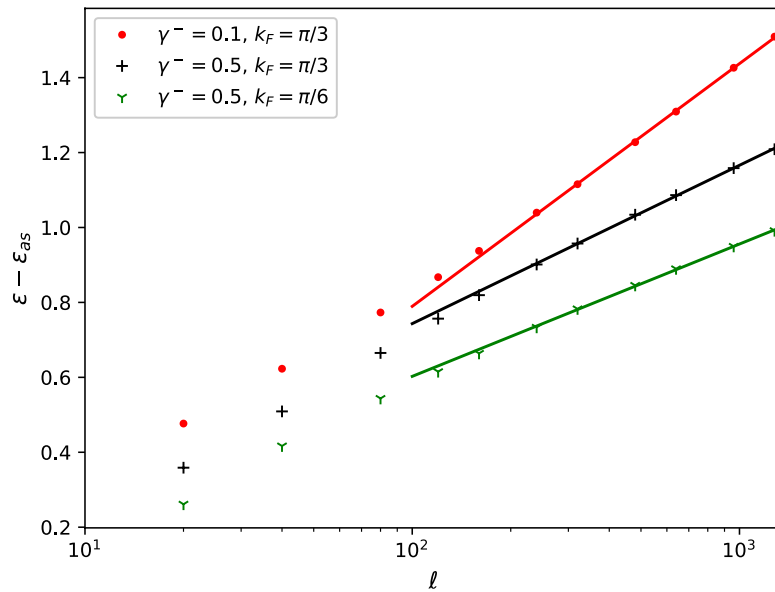


Figure 7. Same as in Fig. 6 using a logarithmic scale on the x -axis. Notice the dependence on the loss rate γ^- of the prefactor of the logarithmic growth.

loss. Our main result is formula (22). Our formula shows that in the standard hydrodynamic limit of large intervals and long times, with their ratio fixed, the fermionic logarithmic negativity between two subsystems placed across the impurity grows linearly with time at short times, and it saturates to a volume-law scaling at asymptotically long times. The genuine entanglement production is traced back to the presence of maximally entangled pairs formed by the reflected and transmitted fermions scattered by the impurity. Although the derivation of (22) is quite involved, we provide a simple physical interpretation in terms of a two-level system for the two intervals. Our formula holds for the geometry with two adjacent intervals, although the generalization to more complicated geometries, such as the one with two disjoint intervals is straightforward.

There are several promising avenues for future research. First, here we considered the paradigmatic setup with a uniform Fermi sea. It would be interesting to consider inhomogeneous initial states [29], and more general localized dissipators, such as gains/losses dissipators. An important question is whether the simple two-level system interpretation of the negativity discussed in section 4 can be generalized. Clearly, it would be interesting to go beyond quadratic dissipative systems, for instance, by considering the effect of localized dephasing or incoherent hopping. The Lindblad equation for both these types of dissipation is integrable by using Bethe ansatz [75, 76]. It would be important to investigate whether integrability persists for local dephasing and incoherent hopping. Our analysis revealed that the fermionic negativity exhibits subleading logarithmic terms besides the leading hydrodynamic one, reflecting that the initial state is critical. It would be interesting to characterize these corrections. This would allow to understand the interplay between dissipation and criticality.

Finally, in our work we considered the dynamical regime in which $\ell, t \rightarrow \infty$ and t/ℓ is fixed. This is only one possibility and several different dynamical regimes can be studied [?]. It would be interesting to characterize the entanglement dynamics in these regimes.

References

- [1] Islam R, Ma R, Preiss P M, Eric Tai M, Lukin A, Rispoli M and Greiner M 2015 *Nature* **528** 77–83 ISSN 1476-4687 URL <https://doi.org/10.1038/nature15750>
- [2] Kaufman A M, Tai M E, Lukin A, Rispoli M, Schittko R, Preiss P M and Greiner M 2016 *Science* **353** 794–800 ISSN 0036-8075 (Preprint <https://science.sciencemag.org/content/353/6301/794.full.pdf>) URL <https://science.sciencemag.org/content/353/6301/794>
- [3] Brydges T, Elben A, Jurcevic P, Vermersch B, Maier C, Lanyon B P, Zoller P, Blatt R and Roos C F 2019 *Science* **364** 260–263 ISSN 0036-8075 (Preprint <https://science.sciencemag.org/content/364/6437/260.full.pdf>) URL <https://science.sciencemag.org/content/364/6437/260>
- [4] Elben A, Kueng R, Huang H Y R, van Bijnen R, Kokail C, Dalmonte M, Calabrese P, Kraus B, Preskill J, Zoller P and Vermersch B 2020 *Phys. Rev. Lett.* **125**(20) 200501 URL <https://link.aps.org/doi/10.1103/PhysRevLett.125.200501>
- [5] Neven A, Carrasco J, Vitale V, Kokail C, Elben A, Dalmonte M, Calabrese P, Zoller P, Vermersch B, Kueng R and Kraus B 2021 *npj Quantum Information* **7** 152 ISSN 2056-6387 URL <https://doi.org/10.1038/s41534-021-00487-y>

- [6] Vitale V, Elben A, Kueng R, Neven A, Carrasco J, Kraus B, Zoller P, Calabrese P, Vermersch B and Dalmonte M 2022 *SciPost Phys.* **12**(3) 106 URL <https://scipost.org/10.21468/SciPostPhys.12.3.106>
- [7] Elben A, Flammia S T, Huang H Y, Kueng R, Preskill J, Vermersch B and Zoller P 2022 The randomized measurement toolbox URL <https://arxiv.org/abs/2203.11374>
- [8] Preskill J 2018 *Quantum* **2** 79 ISSN 2521-327X URL <https://doi.org/10.22331/q-2018-08-06-79>
- [9] Preskill J 2022 The physics of quantum information URL <https://arxiv.org/abs/2208.08064>
- [10] Breuer H P and Petruccione F 2002 *The theory of open quantum systems* (Great Clarendon Street: Oxford University Press)
- [11] Rossini D and Vicari E 2021 *Physics Reports* **936** 1–110 ISSN 0370-1573 URL <https://www.sciencedirect.com/science/article/pii/S0370157321003380>
- [12] Prosen T 2008 *New Journal of Physics* **10** 43026 URL <https://doi.org/10.1088/1367-2630/10/4/043026>
- [13] Alba V and Carollo F 2021 *Phys. Rev. B* **103**(2) L020302 URL <https://link.aps.org/doi/10.1103/PhysRevB.103.L020302>
- [14] Carollo F and Alba V 2022 *Phys. Rev. B* **105**(14) 144305 URL <https://link.aps.org/doi/10.1103/PhysRevB.105.144305>
- [15] Alba V and Carollo F 2022 *Journal of Physics A: Mathematical and Theoretical* **55** 74002 URL <https://doi.org/10.1088/1751-8121/ac48ec>
- [16] Alba V and Carollo F 2022 URL <https://arxiv.org/abs/2205.02139>
- [17] Calabrese P and Cardy J 2005 *Journal of Statistical Mechanics: Theory and Experiment* **2005** P04010 URL <https://doi.org/10.1088/1742-5468/2005/04/P04010>
- [18] Fagotti M and Calabrese P 2008 *Phys. Rev. A* **78**(1) 010306 URL <https://link.aps.org/doi/10.1103/PhysRevA.78.010306>
- [19] Alba V and Calabrese P 2017 *Proceedings of the National Academy of Sciences* **114** 7947–7951 ISSN 0027-8424 (*Preprint* <https://www.pnas.org/content/114/30/7947.full.pdf>) URL <https://www.pnas.org/content/114/30/7947>
- [20] Alba V and Calabrese P 2018 *SciPost Phys.* **4**(3) 17 URL <https://scipost.org/10.21468/SciPostPhys.4.3.017>
- [21] Alba V, Bertini B, Fagotti M, Piroli L and Ruggiero P 2021 *Journal of Statistical Mechanics: Theory and Experiment* **2021** 114004 URL <https://doi.org/10.1088/1742-5468/ac257d>
- [22] Vidal G and Werner R F 2002 *Phys. Rev. A* **65**(3) 032314 URL <https://link.aps.org/doi/10.1103/PhysRevA.65.032314>
- [23] Shapourian H and Ryu S 2019 *Phys. Rev. A* **99**(2) 022310 URL <https://link.aps.org/doi/10.1103/PhysRevA.99.022310>
- [24] Alba V 2022 *SciPost Phys.* **12**(1) 11 URL <https://scipost.org/10.21468/SciPostPhys.12.1.011>
- [25] Eisler V and Peschel I 2012 *EPL (Europhysics Letters)* **99** 20001
- [26] Gruber M and Eisler V 2020 *Journal of Physics A: Mathematical and Theoretical* **53** 205301
- [27] Fraenkel S and Goldstein M 2022 Extensive Long-Range Entanglement in a Nonequilibrium Steady State URL <https://arxiv.org/abs/2205.12991>
- [28] Alba V and Calabrese P 2019 *EPL (Europhysics Letters)* **126** 60001 URL <https://doi.org/10.1209/0295-5075/126/60001>
- [29] Alba V and Carollo F 2022 *Phys. Rev. B* **105**(5) 054303 URL <https://link.aps.org/doi/10.1103/PhysRevB.105.054303>
- [30] Peschel I and Eisler V 2009 *Journal of physics a: mathematical and theoretical* **42** 504003
- [31] Krapivsky P L, Mallick K and Sels D 2019 *Journal of Statistical Mechanics: Theory and Experiment* **2019** 113108 URL <https://doi.org/10.1088/1742-5468/2019/04/113108>
- [32] Burke P C, Wiersig J and Haque M 2020 *Phys. Rev. A* **102**(1) 012212 URL <https://link.aps.org/doi/10.1103/PhysRevA.102.012212>

- [33] Shapourian H, Shiozaki K and Ryu S 2017 *Phys. Rev. Lett.* **118**(21) 216402 URL <https://link.aps.org/doi/10.1103/PhysRevLett.118.216402>
- [34] Shapourian H, Shiozaki K and Ryu S 2017 *Phys. Rev. B* **95**(16) 165101 URL <https://link.aps.org/doi/10.1103/PhysRevB.95.165101>
- [35] Shapourian H and Ryu S 2019 *Journal of Statistical Mechanics: Theory and Experiment* **2019** 43106 URL <https://doi.org/10.1088/1742-5468/ab11e0>
- [36] Eisert J and Plenio M B 1999 *Journal of Modern Optics* **46** 145–154 (Preprint <https://www.tandfonline.com/doi/pdf/10.1080/09500349908231260>) URL <https://www.tandfonline.com/doi/abs/10.1080/09500349908231260>
- [37] Plenio M B 2005 *Phys. Rev. Lett.* **95**(9) 090503 URL <https://link.aps.org/doi/10.1103/PhysRevLett.95.090503>
- [38] Wichterich H, Molina-Vilaplana J and Bose S 2009 *Phys. Rev. A* **80**(1) 010304 URL <https://link.aps.org/doi/10.1103/PhysRevA.80.010304>
- [39] Calabrese P, Cardy J and Tonni E 2012 *Phys. Rev. Lett.* **109**(13) 130502 URL <https://link.aps.org/doi/10.1103/PhysRevLett.109.130502>
- [40] Eisler V and Zimborás Z 2015 *New Journal of Physics* **17** 053048 URL <https://doi.org/10.1088/1367-2630/17/5/053048>
- [41] Herzog C P and Wang Y 2016 *Journal of Statistical Mechanics: Theory and Experiment* **2016** 073102 URL <https://doi.org/10.1088/1742-5468/2016/07/073102>
- [42] Audenaert K, Eisert J, Plenio M B and Werner R F 2002 *Phys. Rev. A* **66**(4) 042327 URL <https://link.aps.org/doi/10.1103/PhysRevA.66.042327>
- [43] Calabrese P, Cardy J and Tonni E 2013 *Journal of Statistical Mechanics: Theory and Experiment* **2013** P02008
- [44] Blondeau-Fournier O, Castro-Alvaredo O A and Doyon B 2016 *Journal of Physics A: Mathematical and Theoretical* **49** 125401 URL <https://doi.org/10.1088/1751-8113/49/12/125401>
- [45] Hoogeveen M and Doyon B 2015 *Nuclear Physics B* **898** 78–112 ISSN 0550-3213 URL <https://www.sciencedirect.com/science/article/pii/S0550321315002242>
- [46] Ruggiero P, Alba V and Calabrese P 2016 *Phys. Rev. B* **94**(19) 195121 URL <https://link.aps.org/doi/10.1103/PhysRevB.94.195121>
- [47] Shapourian H, Ruggiero P, Ryu S and Calabrese P 2019 *SciPost Phys.* **7** 037 URL <https://scipost.org/10.21468/SciPostPhys.7.3.037>
- [48] Ruggiero P, Alba V and Calabrese P 2016 *Phys. Rev. B* **94**(3) 035152 URL <https://link.aps.org/doi/10.1103/PhysRevB.94.035152>
- [49] Wald S, Arias R and Alba V 2020 *Journal of Statistical Mechanics: Theory and Experiment* **2020** ISSN 17425468
- [50] Lu T C and Grover T 2020 *Phys. Rev. B* **102**(23) 235110 URL <https://link.aps.org/doi/10.1103/PhysRevB.102.235110>
- [51] Wu K H, Lu T C, Chung C M, Kao Y J and Grover T 2020 *Phys. Rev. Lett.* **125**(14) 140603 URL <https://link.aps.org/doi/10.1103/PhysRevLett.125.140603>
- [52] Calabrese P, Essler F H L and Mussardo G 2016 *Journal of Statistical Mechanics: Theory and Experiment* **2016** 064001 URL <https://doi.org/10.1088/1742-5468/2016/06/064001>
- [53] Coser A, Tonni E and Calabrese P 2014 *Journal of Statistical Mechanics: Theory and Experiment* **2014** P12017 URL <https://doi.org/10.1088/1742-5468/2014/12/p12017>
- [54] Wen X, Chang P Y and Ryu S 2015 *Phys. Rev. B* **92**(7) 075109 URL <https://link.aps.org/doi/10.1103/PhysRevB.92.075109>
- [55] Kudler-Flam J, Kusuki Y and Ryu S 2020 *Journal of High Energy Physics* **2020** 74 ISSN 1029-8479 URL [https://doi.org/10.1007/JHEP04\(2020\)074](https://doi.org/10.1007/JHEP04(2020)074)
- [56] Kudler-Flam J, Kusuki Y and Ryu S 2021 *Journal of High Energy Physics* **2021** 146 ISSN 1029-8479 URL [https://doi.org/10.1007/JHEP03\(2021\)146](https://doi.org/10.1007/JHEP03(2021)146)
- [57] Klobas K, Bertini B and Piroli L 2021 *Phys. Rev. Lett.* **126**(16) 160602 URL <https://link.aps.org/doi/10.1103/PhysRevLett.126.160602>

- [58] Klobas K and Bertini B 2021 *SciPost Phys.* **11**(6) 107 URL <https://scipost.org/10.21468/SciPostPhys.11.6.107>
- [59] Murciano S, Alba V and Calabrese P 2021 Quench dynamics of Rényi negativities and the quasiparticle picture (*Preprint* [arXiv:2110.14589](https://arxiv.org/abs/2110.14589))
- [60] Ruggiero P and Turkeshi X 2022 URL <https://arxiv.org/abs/2206.02934>
- [61] Carollo F and Alba V 2022 Entangled multiplets and unusual spreading of quantum correlations in a continuously monitored tight-binding chain URL <https://arxiv.org/abs/2206.07806>
- [62] Turkeshi X, Piroli L and Schiró M 2022 *Phys. Rev. B* **106**(2) 024304 URL <https://link.aps.org/doi/10.1103/PhysRevB.106.024304>
- [63] Collura M and Calabrese P 2013 *Journal of Physics A: Mathematical and Theoretical* **46** 175001
- [64] Gamayun O, Slobodeniuk A, Caux J S and Lychkovskiy O 2021 *Phys. Rev. B* **103**(4) L041405 URL <https://link.aps.org/doi/10.1103/PhysRevB.103.L041405>
- [65] Gamayun O, Lychkovskiy O and Caux J S 2020 *SciPost Phys.* **8**(3) 36 URL <https://scipost.org/10.21468/SciPostPhys.8.3.036>
- [66] Capizzi L and Eisler V 2022 URL <https://arxiv.org/abs/2209.03297>
- [67] Alba V and Calabrese P 2018 *SciPost Phys.* **4**(3) 17 URL <https://scipost.org/10.21468/SciPostPhys.4.3.017>
- [68] Alba V and Calabrese P 2017 *Phys. Rev. B* **96**(11) 115421 URL <https://link.aps.org/doi/10.1103/PhysRevB.96.115421>
- [69] Bertini B, Klobas K, Alba V, Lagnese G and Calabrese P 2022 *Phys. Rev. X* **12**(3) 031016 URL <https://link.aps.org/doi/10.1103/PhysRevX.12.031016>
- [70] Wong R 2001 *Asymptotic Approximations of Integrals* (Society for Industrial and Applied Mathematics) URL <https://epubs.siam.org/doi/abs/10.1137/1.9780898719260>
- [71] Degasperis A, Fonda L and Ghirardi G C 1974 *Il Nuovo Cimento A (1965-1970)* **21** 471–484 ISSN 1826-9869 URL <https://doi.org/10.1007/BF02731351>
- [72] Misra B and Sudarshan E C G 1977 *Journal of Mathematical Physics* **18** 756–763 URL <https://doi.org/10.1063/1.523304>
- [73] Facchi P and Pascazio S 2002 *Phys. Rev. Lett.* **89**(8) 080401 URL <https://link.aps.org/doi/10.1103/PhysRevLett.89.080401>
- [74] Di Francesco P, Mathieu P and Senechal D 1997 *Conformal Field Theory* Graduate Texts in Contemporary Physics (New York: Springer-Verlag) ISBN 978-0-387-94785-3, 978-1-4612-7475-9
- [75] Eisler V 2011 *Journal of Statistical Mechanics: Theory and Experiment* **2011** P06007 URL <https://doi.org/10.1088/1742-5468/2011/06/p06007>
- [76] Medvedyeva M V, Essler F H L and Prosen T 2016 *Phys. Rev. Lett.* **117**(13) 137202 URL <https://link.aps.org/doi/10.1103/PhysRevLett.117.137202>

Appendix A. Hydrodynamic prediction for the negativity: Derivation of Eq. (22)

Let us consider the case of the two symmetric intervals A_1 and A_2 , with $A_1 = [1, \ell]$ and $A_2 = [-\ell, -1]$ as our subsystems (see Fig. 1). The covariance matrix G (cf. (6)) has the structure:

$$G = \begin{pmatrix} G^{11} & G^{12} \\ G^{21} & G^{22} \end{pmatrix} = \begin{pmatrix} G_{x,y} & G_{x,-y} \\ G_{-x,y} & G_{-x,-y} \end{pmatrix}, \quad x, y \in [1, \ell]. \quad (\text{A.1})$$

In the same way and following section 3, we can use (A.1) in the definition of the matrix $\Gamma = \mathbf{1} - 2G$ (cf. (16)) as

$$\Gamma_{x,y}^{\pm} := 2 \begin{pmatrix} G_{x,y} & \mp i G_{x,-y} \\ \mp i G_{-x,y} & -G_{-x,-y} \end{pmatrix} - \delta_{x,y} \sigma_z, \quad x, y \in [1, \ell], \quad (\text{A.2})$$

where σ_z is the Pauli matrix. We observe that $\Gamma^+ + \Gamma^-$ is block diagonal, i.e.,

$$\Gamma_{x,y}^+ + \Gamma_{x,y}^- = 4 \begin{pmatrix} G_{x,y} & 0 \\ 0 & -G_{-x,-y} \end{pmatrix} - 2\delta_{x,y} \sigma_z. \quad (\text{A.3})$$

Using the definition of $G_{x,y}$ (cf. (6)), we can now write $\Gamma_{x,y}^{\pm}$ as

$$\Gamma_{x,y}^{\pm} = 2 \int_{-k_F}^{k_F} \frac{dk}{2\pi} \begin{pmatrix} S_{k,x} \\ \mp i S_{-k,x} \end{pmatrix} (\bar{S}_{k,y} \quad \mp i \bar{S}_{-k,y}) - \delta_{x,y} \sigma_z \quad (\text{A.4})$$

where $S_{k,x}$ and $S_{k,y}$ are defined in (10). We also have

$$\Gamma_{x,y}^+ + \Gamma_{x,y}^- = 4 \int_{-k_F}^{k_F} \frac{dk}{2\pi} \begin{pmatrix} S_{k,x} \bar{S}_{k,y} & 0 \\ 0 & -S_{-k,x} \bar{S}_{-k,y} \end{pmatrix} - 2\delta_{x,y} \sigma_z \quad (\text{A.5})$$

where we used the fact that $S_{k,-x} = S_{-k,x}$, which is apparent from (10).

To compute the fermionic negativity, it is necessary to evaluate the moments of the correlators $M_p(\{n_j\})$ defined as

$$M_p(\{n_j\}) = \text{Tr} \left[\prod_{j=1}^p (\Gamma^+ \Gamma^-)^{n_j} (\Gamma^+ + \Gamma^-) \right]. \quad (\text{A.6})$$

Here n_j with $j = 1, \dots, p$ is a positive integer. The matrices Γ^{\pm} appearing in (A.6) are restricted to subsystem A , i.e., they are $2\ell \times 2\ell$ matrices. Moreover, M_p depends on time. Here we are interested in the hydrodynamic limit, which is defined as the limit $t, \ell \rightarrow \infty$, with the ratio t/ℓ fixed. Terms of the form (A.7) are obtained from the series representation of the matrix Ξ (cf. (19)).

Appendix A.1. Truncated moments

To proceed, it is crucial to observe that Γ^{\pm} (cf. (A.2)) consists of the sum of two terms. The first one depends on $S_{k,x}$ (see (10) and (A.4)), whereas the second one is $\delta_{x,y} \sigma_z$ and does not depend on the quasimomenta. For now, in multiplying the matrices Γ^{\pm} in (A.6), we are going to neglect the term σ_z in (A.2). Let us define these ‘‘truncated’’ moments as M_p^t . They are defined as

$$M_p^t(\{n_j\}) = \text{Tr} \left[\prod_{j=1}^p (\Gamma^+ \Gamma^-)^{n_j} (\Gamma^+ + \Gamma^-) \right]^t, \quad (\text{A.7})$$

where the superscript t in the right hand side is to stress that we neglect the term $\delta_{x,y} \sigma_z$ in the definition of Γ^{\pm} (cf. (A.2)). The trace in (A.7) is performed over both the spatial

indices as well as over the indices of the 2×2 block matrix. After performing the trace over the latter, a simple structure arises. Precisely, upon expanding the product in (A.7) one obtains a string of operators Γ^\pm , which gives rise to strings of $S_{k,x}$. The strings of $S_{k,x}$ are constructed following three rules that we now discuss. Let us consider a generic string \mathcal{S} of operators as

$$\mathcal{S} = (\Gamma^+\Gamma^-)^{n_1}(\Gamma^+ + \Gamma^-)(\Gamma^+\Gamma^-)^{n_2}\dots(\Gamma^+\Gamma^-)^{n_p}(\Gamma^+ + \Gamma^-). \quad (\text{A.8})$$

Let us recall that each Γ^\pm contains an integral over one of the quasimomenta k_j (cf. (A.2)), with k_1 the quasimomentum associated with the leftmost Γ^+ in the string (A.8), and k_{2N_p+p} the one associated with the last term $(\Gamma^+ + \Gamma^-)$. The rules to expand (A.8) in terms of strings of $S_{k,x}$ (cf. (10)) are the following.

- (i) There is an overall factor 2^{2N_p+2p} , with $N_p = \sum_j n_j$, and a multidimensional integral over the quasimomenta k_j , with $j = 1, 2, \dots, 2N_p + p$ as

$$M_p^t \rightarrow 2^{2N_p+2p} \int_{-k_F}^{k_F} \frac{d^{2N_p+p}k}{(2\pi)^{2N_p+p}} I(\{k_j\}), \quad (\text{A.9})$$

where $I(\{k_j\})$ is determined from (A.8) by rules (ii) and (iii) below.

- (ii) Every couple of neighbouring operators $\Gamma_{x_1,x_2}^+(k_1)\Gamma_{x_2,x_3}^-(k_2)$ or $\Gamma_{x_1,x_2}^-(k_1)\Gamma_{x_2,x_3}^+(k_2)$ that one encounters by scanning site by site the string \mathcal{S} in (A.8) from left to right contributes with a term $(\bar{S}_{k_1,x_2}S_{k_2,x_2} + \bar{S}_{-k_1,x_2}S_{-k_2,x_2})$ to the integrand $I(\{k_j\})$ in (A.9) (cf. (A.4)).
- (iii) Each sequence of the type $\Gamma_{x_1,x_2}^-(k_1)(\Gamma_{x_2,x_3}^+(k_2) + \Gamma_{x_2,x_3}^-(k_2))\Gamma_{x_3,x_4}^+(k_3)$ that one can identify in \mathcal{S} contributes with a term $(\bar{S}_{k_1,x_2}S_{k_2,x_2}\bar{S}_{k_2,x_3}S_{k_3,x_3} - \bar{S}_{-k_1,x_2}S_{-k_2,x_2}\bar{S}_{-k_2,x_3}S_{-k_3,x_3})$ in $I(\{k_j\})$ (see (A.4) and (A.5)).

In rule (ii) and (iii) we sum over repeated spatial indices x_j . Notice also that the symbol $\Gamma^\pm(k_j)$ with the argument k_j denotes the integrand in the definition of Γ^\pm (cf. (A.4)) and k_j is the integration variable. Let us check the combined effect of rule (ii) and (iii) by considering the case with $p = 2$ and $n_1 = n_2 = 1$ in (A.7). The string \mathcal{S} in (A.8) becomes

$$\begin{aligned} \mathcal{S} = & \Gamma_{x_1,x_2}^+(k_1)\Gamma_{x_2,x_3}^-(k_2)(\Gamma_{x_3,x_4}^+(k_3) + \Gamma_{x_3,x_4}^-(k_3)) \\ & \times \Gamma_{x_4,x_5}^+(k_4)\Gamma_{x_5,x_6}^-(k_5)(\Gamma_{x_6,x_1}^+(k_6) + \Gamma_{x_6,x_1}^-(k_6)). \end{aligned} \quad (\text{A.10})$$

The application of rule (ii) and (iii) gives

$$\begin{aligned} M_2^t \rightarrow & (\bar{S}_{k_1,x_2}S_{k_2,x_2} + \bar{S}_{-k_1,x_2}S_{-k_2,x_2})(\bar{S}_{k_2,x_3}S_{k_3,x_3}\bar{S}_{k_3,x_4}S_{k_4,x_4} - \bar{S}_{-k_2,x_3}S_{-k_3,x_3}\bar{S}_{-k_3,x_4}S_{-k_4,x_4}) \\ & (\bar{S}_{k_4,x_5}S_{k_5,x_5} + \bar{S}_{-k_4,x_5}S_{-k_5,x_5})(\bar{S}_{k_5,x_6}S_{k_6,x_6}\bar{S}_{k_6,x_1}S_{k_1,x_1} - \bar{S}_{-k_5,x_6}S_{-k_6,x_6}\bar{S}_{-k_6,x_1}S_{-k_1,x_1}) \end{aligned} \quad (\text{A.11})$$

Again, in (A.10) and (A.11) repeated spatial indices are summed over. As it is clear from (A.11), the effect of the operators $(\Gamma^+ + \Gamma^-)$ is to introduce the minus signs in the

terms in the round brackets. This is due to the fact that upon expanding Eq. (A.10) there are terms with “defects”, i.e., that contain the same operators on consecutive places. Before proceeding, it is useful to notice that if p in (A.7) is odd, the integration of the resulting product vanishes. Indeed, the integration domain is invariant under the transformation $k_i \rightarrow -k_i \forall i$, while the integrand is odd under this transformation. This happens because rule (iii) provides p terms which are odd, while rule (ii) give only even terms. To perform the summation over the spatial indices, we use the identity

$$\sum_{z=1}^{\ell} e^{izk} = \frac{\ell}{4} \int_{-1}^1 d\xi \frac{k}{\sin(k/2)} e^{i(\ell\xi+\ell+1)k/2}. \quad (\text{A.12})$$

It allows to rewrite the correlator (A.7) as an integral in $2N_p + p$ ξ -variables, alongside an equal number of quasimomentum k -variables. We obtain, for the generic case:

$$\begin{aligned} M_p^t = & \left(\frac{\ell}{2}\right)^{2N_p+p} \int_{-k_F}^{k_F} \frac{d^{2N_p+p}k}{(2\pi)^{2N_p+p}} \int_{-1}^1 d^{2N_p+p}\xi \\ & \sum_{\text{signs}} \sum_{\sigma_j, \tau_j=0,1} \prod_{i=1}^p \left[\left(\prod_{j=2N_{i-1}+i}^{J_i=2N_i+i-1} e^{i\ell(\xi_j+1)([\pm k]_{\sigma_j}-[\pm k]_{\tau_{j-1}})/2} \tilde{\gamma}^{\sigma_j} \tilde{\gamma}^{\tau_{j-1}} \right) \right. \\ & \left. \times \left\{ (\pm 1) e^{i\ell(\xi_{J_i+1}+1)([\pm k]_{\sigma_{J_i+1}}-[\pm k]_{\tau_{J_i}})/2} e^{i\ell(\xi_{J_i+2}+1)([\pm k]_{\sigma_{J_i+2}}-[\pm k]_{\tau_{J_i+1}})/2} \tilde{\gamma}^{\sigma_{J_i+1}} \tilde{\gamma}^{\tau_{J_i}} \tilde{\gamma}^{\sigma_{J_i+2}} \tilde{\gamma}^{\tau_{J_i+1}} \right\} \right], \end{aligned} \quad (\text{A.13})$$

where we defined $N_i := \sum_{j=1}^i n_j$ (cf. (A.7)), and

$$[k]_{\sigma_j} = \begin{cases} k_j & \sigma_j = 0 \\ |k_j| & \sigma_j = 1 \end{cases} \quad (\text{A.14})$$

Moreover, we defined \tilde{r} as

$$\tilde{r}^{\sigma_j} := \left(r(k_j) \Theta(-\ell(\xi_j + 1)/2 + |v_{k_j}|t) \right)^{\sigma_j}. \quad (\text{A.15})$$

Here $r(k_j)$ is the reflection coefficient in (11). Finally, in (A.13) we sum over the \pm signs in the term within the square brackets. Importantly, all the signs in the underlined term in the curly brackets in (A.13) have to be equal.

Let us now discuss the structure of (A.13). The integration in ξ_j originates from the application of (A.12) to treat the matrix multiplications and the trace in (A.7). Crucially, in applying (A.12) we used that in the hydrodynamic limit $\ell, t \rightarrow \infty$ with their ratio t/ℓ fixed, the stationary phase approximation for the integral in (A.13) gives as stationary point $k_j \rightarrow \pm k_1$ for each j . Moreover, we used that the integral in dq in the definition of $S_{k,x}$ (cf. (14)) is dominated by $q \rightarrow 0$. This implies that we can replace $k/\sin(k/2) \rightarrow 2$ in (A.12). We can also perform the integrations over q , which after using the identity

$$\int_{-\infty}^{\infty} \frac{dq}{2\pi i} \frac{e^{iqx}}{q - i0} = \Theta(x), \quad (\text{A.16})$$

give the terms with \tilde{r} (cf. (A.15)) in (A.13).

The sum over the variables σ_j, τ_j in (A.13) takes into account that each $S_{k,x}$ (cf. (14)) contains a term that depends on k_j and one that depends on $|k_j|$. The latter is associated with a factor $\tilde{r}(k_j)$. The sum over the signs of k_j reflects that for each term $S_{k,x}$ in (A.7) there is a term with $S_{-k,x}$ (see, for instance, Eq. (A.11) for the case with $p = 2$). The signs in the second row of (A.13) can be chosen independently for each exponential in the product, as rule (ii) yields two possible factors with opposite quasi-momentum, while in the underlined term in (A.13) all the signs have to be equal, following from rule (iii). Indeed, in rule (iii) the terms $S_{k,x}$ with the minus sign have also the two quasimomenta reversed.

To illustrate the structure of (A.13) let us consider again the case with $p = 2$ and $n_1 = n_2 = 1$. Now, Eq. (A.13) becomes

$$\begin{aligned}
 M_2^t(1, 1) = & \\
 \left(\frac{\ell}{2}\right)^6 \sum_{\text{signs}} \int_{-k_F}^{k_F} \frac{d^6 k}{(2\pi)^6} \int_{-1}^1 d^6 \xi \sum_{\sigma_j, \tau_j} & e^{i\ell(\xi_2+1)([\pm k]_{\sigma_2}-[\pm k]_{\tau_1})+i\ell(\xi_5+1)([\pm k]_{\sigma_5}-[\pm k]_{\tau_4})} \tilde{r}^{\sigma_2} \tilde{r}^{\tau_1} \tilde{r}^{\sigma_5} \tilde{r}^{\tau_4} \\
 & \{(\pm 1)e^{i\ell(\xi_3+1)([\pm k]_{\sigma_3}-[\pm k]_{\tau_2})+i\ell(\xi_4+1)([\pm k]_{\sigma_4}-[\pm k]_{\tau_3})} \tilde{r}^{\sigma_4} \tilde{r}^{\sigma_3} \tilde{r}^{\tau_2} \tilde{r}^{\tau_3}\} \\
 & \{(\pm 1)e^{+i\ell(\xi_6+1)([\pm k]_{\sigma_6}-[\pm k]_{\tau_5})+i\ell(\xi_1+1)([\pm k]_{\sigma_1}-[\pm k]_{\tau_6})} \tilde{r}^{\sigma_6} \tilde{r}^{\sigma_1} \tilde{r}^{\tau_5} \tilde{r}^{\tau_6}\} \quad (\text{A.17})
 \end{aligned}$$

Let us now perform the stationary phase analysis in the limit $\ell, t \rightarrow \infty$ with their ratio t/ℓ fixed. Here we perform the stationary phase approximation with respect to both variables k_j and ξ_j . Before proceeding, let us restrict ourselves to the case in which the variables τ_j, σ_j are not all zero. The configuration with $\sigma_j = \tau_j = 0, \forall j$ will be discussed at the end. First, we notice that all the quasimomenta appear twice in the phase factors in (A.13), as it is also clear from (A.17) (notice the presence of the terms $[\pm k]_{\sigma_j}$ and $[\pm k]_{\tau_j}$). Let us define the two indices (σ_j, τ_j) as *paired* if $\sigma_j = \tau_j = 1$, and *unpaired* otherwise. Moreover, we observe that we can treat the terms arising from the operators $\dots(\Gamma^+ + \Gamma^-)\dots$ and $\dots(\Gamma^+\Gamma^-)^{n_j}\dots$ separately. Let us start discussing the first ones, which corresponds to the underlined terms in the curly brackets in (A.13). Now, the signs \pm of two occurrences of k_j have to be the same because both occurrences of k_j are in the same underlined block. This is also clear in (A.17) for $p = 2$. The two occurrences of the quasimomenta k_3 and k_6 appear with the same sign.

It is straightforward to check that if one has $\sigma_j = 0$ or $\tau_j = 0$, i.e., if the (σ_j, τ_j) are not paired, then the stationarity condition with respect to k_j fixes the sign of k_j . Specifically, one has that $k_j > 0$ if the chosen sign in the curly bracket to which k_j belongs is plus, and minus otherwise. This follows from the requirement that the solution of the stationarity condition for ξ_i belongs to the integration domain $[-1, 1] \forall i$. On the other hand, if the indices (σ_j, τ_j) are paired, then the sign of k_j is not fixed, i.e., $k_j \in [-k_F, k_F]$. Since the integrand is symmetric under exchange $k_j \rightarrow -k_j$, the difference between paired and unpaired indices is a factor two. Now, the calculation of the contribution of the terms in the curly brackets in (A.13) involves some elementary combinatorics, and it is the same as in Ref. [24]. For now, we also omit the step function in (A.15). In summary,

the result is

$$\cdots(\Gamma^+ + \Gamma^-)\cdots \rightarrow (1 + 2r + 2r^2)^p = (1 - |a(k)|^2)^p \quad (\text{A.18})$$

In (A.18) $|a(k)|^2$ is the absorption coefficient (13), and we are using that in the stationary phase approximation $k_j = \pm k$ for any j and that $|a(k)|^2 = |a(-k)|^2$.

Let us now discuss the contribution of the terms $\cdots(\Gamma^+\Gamma^-)^{n_j}\cdots$ in (A.8). Now the pairs of momenta appearing in the generic block $(\Gamma^+\Gamma^-)^{n_j}$ are not forced to have the same sign. Again, this is clear by considering the toy example with $p = 2$ and $n_1 = n_2 = 1$ in (A.17). In principle, one has to sum over the plus and minus signs in $[\pm k]_{\sigma_j}$ and $[\pm k]_{\tau_j}$. The result depends on the choice of sign of the quasimomenta at the edges of the block. Let us first consider the case in which the quasimomenta at the edges have the same sign. Let us also start from the case in which all the σ_j and τ_j associated with quasimomenta in the block are zero. Now, it is easy to convince oneself that stationarity with respect to k_j implies that there is only one allowed sign configuration, which gives result 1. It is also not difficult to check that if there is at least a σ_j or a τ_j equal to 1 there is a factor 2^{i-1} , where i is the number of indices σ_j, τ_j that are equal to 1. By summing over σ_j, τ_j , one obtains Z_{2n_j} , where

$$Z_n := \sum_{i=1}^{2n} \binom{2n}{i} 2^{i-1} r^i = \frac{(1 + 2r)^{2n} - 1}{2} = \frac{(1 - 2|a|^2)^n - 1}{2} \quad (\text{A.19})$$

Thus, the total result is $1 + Z_{2n_j}$. Instead, if the signs of the quasimomenta at the edges are different, the result is Z_{2n_j} , since there is no stationary phase contribution from the case of all the σ_j, τ_j in the block equal to zero.

Finally, we have to glue together the contributions of the different blocks $\cdots(\Gamma^+\Gamma^-)^{n_j}$ with different j . It is easy to show that the final result is

$$\prod_{j=1}^p (\cdots(\Gamma^+\Gamma^-)^{n_j}\cdots) \rightarrow \text{Tr} \left[\prod_{j=1}^p \begin{pmatrix} 1 + Z_{2n_j} & -Z_{2n_j} \\ Z_{2n_j} & -1 - Z_{2n_j} \end{pmatrix} \right] \quad (\text{A.20})$$

where Z_{2n_j} is defined in (A.19). The minus sign in the second column is the minus sign that appears in the terms with reversed quasimomenta in rule (iii). Notice that if $n_j = 0$, $Z_{2n_j} = 0$ and there are no configurations with different sign at the endpoints, as it should be: $n_j = 0$ implies the presence of two consecutive $(\Gamma^+ + \Gamma^-)$ factors. Putting all together, we obtain the final result for M_p^t with even p as

$$M_p^t = 2^{2(N_p+p)-1} \int_{-k_F}^{k_F} \frac{dk}{2\pi} \left\{ 4\ell + \min(|v_k|t, \ell) \left((1 - |a|^2)^p \text{Tr} \left[\prod_{i=1}^p \begin{pmatrix} 1 + Z_{2n_i} & -Z_{2n_i} \\ Z_{2n_i} & -1 - Z_{2n_i} \end{pmatrix} \right] - 2 \right) \right\}. \quad (\text{A.21})$$

The term $\min(|v_k|t, \ell)$ comes from the final integration of the step function in (A.15) that one has to perform every time there is at least a σ_j or a τ_j equal to 1, in the same way as explained in [24]. The two configurations we have for $\sigma_j = \tau_j = 0 \quad \forall j$ (the signs all equal to plus or to minus) must be subtracted from the combinatorial factor and treated separately, yielding the term 4ℓ in (A.21).

Appendix A.2. Full moments

We now consider the full moments M_p , taking into account the terms $\delta_{x,y}\sigma_z$ in the definition of $G_{x,y}$ (cf. (17)). This means that we are allowed to replace any occurrence of $G_{x,y}$ with $-\delta_{x,y}\sigma_z$ in each Γ^\pm correlator. It is easy to check that by substituting a term $-\delta_{x,y}\sigma_z$ in a block $(\Gamma^+\Gamma^-)^{n_j}$ the structure of the calculation remains the same as in the previous section. The result differs from (A.20) by a factor $-1/2$ and by the substitution $Z_{2n_j} \rightarrow Z_{2n_j-1}$. In a similar way, the replacement of a $G_{x,y}$ in a term like $(\Gamma^+ + \Gamma^-)$ gives an overall $-1/2$ and the substitution $(1 - |a^2|)^p \rightarrow (1 - |a^2|)^{p-1}$ in (A.18). So in the end Eq. (A.21) becomes

$$M_p = \text{Tr} \prod_{j=1}^p [(\Gamma^+\Gamma^-)^{n_j} (\Gamma^+ + \Gamma^-)] = \sum_{i=0}^p \binom{p}{i} 4^{p-i} (-2)^i \prod_{l=1}^p \sum_{j_l=0}^{2n_l} \binom{2n_l}{j_l} 2^{2n_l-j_l} (-1)^{j_l} \\ \times \left(\frac{\ell}{2}\right) \int_{-k_F}^{k_F} \frac{dk}{2\pi} \left\{ 4 + \min(|v_k|t/\ell, 1) \left((1 - |a^2|)^{p-i} \text{Tr} \left[\prod_{h=1}^p \begin{pmatrix} 1 + Z_{2n_h-j_h} & -Z_{2n_h-j_h} \\ Z_{2n_h-j_h} & -1 - Z_{2n_h-j_h} \end{pmatrix} \right] - 2 \right) \right\}. \quad (\text{A.22})$$

Here the first sum takes into account the different ways of inserting the term σ_z in strings of the type $\dots(\Gamma^+ + \Gamma^-)\dots$. The second sum accounts for insertions in blocks of the type $\dots(\Gamma^+\Gamma^-)^{n_j}\dots$. This holds for p even, while for odd p every term in the sum is still zero, for the same symmetry reasons as above. Before proceeding, we notice that in (A.22) the term with $i = p$ and $j_m = 2n_m$ has to be treated separately. It corresponds to replacing all the occurrences of the operators Γ^\pm with $\Gamma_{x,y}^\pm \sim \delta_{x,y}\sigma_z$. This term gives 2ℓ . Now, after performing the sums in (A.22), we obtain:

$$M_p = 2^p \int_{-k_F}^{k_F} \frac{dk}{2\pi} \left\{ \frac{2\pi\ell}{k_F} + \min(|v_k|t, \ell) \left(\frac{1}{2} (1 - 2|a^2|)^p \text{Tr} \left[\prod_{h=1}^p \begin{pmatrix} 1 + \tilde{Z}_{2n_h} & -\tilde{Z}_{2n_h} \\ \tilde{Z}_{2n_h} & -1 - \tilde{Z}_{2n_h} \end{pmatrix} \right] - 1 \right) \right\}, \quad (\text{A.23})$$

where we have defined:

$$\tilde{Z}_n := \frac{(1 - 4|a^2|)^n - 1}{2}. \quad (\text{A.24})$$

The first term in the square brackets in (A.23) corresponds to $i = p$ and $j_m = 2n_m$.

Eq. (A.23) provides the building block to compute terms \widetilde{M}_p of the form

$$\widetilde{M}_p := \text{Tr} \left[(P^{-1}(\Gamma^+ + \Gamma^-))^p \right], \quad (\text{A.25})$$

where $P = \mathbf{1} + \Gamma^+\Gamma^-$. These terms are needed to compute the negativity (18). The strategy to compute (A.25) is to use the trivial identity

$$P^{-1} = \sum_{n=0}^{\infty} (-1)^n (\Gamma^+\Gamma^-)^n. \quad (\text{A.26})$$

We can rewrite (A.25) as

$$\widetilde{M}_p = \text{Tr} \left[\prod_{j=1}^p \left(\sum_{n_j=0}^{\infty} (-1)^{n_j} (\Gamma^+\Gamma^-)^{n_j} (\Gamma^+ + \Gamma^-) \right) \right]. \quad (\text{A.27})$$

Now we can apply the result (A.23) to each term in (A.27). By using the regularisation $\sum_{n=0}^{\infty} (-1)^n = \frac{1}{2}$, we obtain:

$$\begin{aligned} \widetilde{M}_p &= \int_{-k_F}^{k_F} \frac{dk}{2\pi} \left\{ \frac{2\pi\ell}{k_F} - \min(|v_k|t, \ell) + 2^{p-1} \min(|v_k|t, \ell) (1 - 2|a|^2)^p \text{Tr} \left[\begin{pmatrix} 1/2 + b & -b \\ b & -1/2 - b \end{pmatrix}^p \right] \right\} = \\ &= \int_{-k_F}^{k_F} \frac{dk}{2\pi} \left[\frac{2\pi\ell}{k_F} - \min(|v_k|t, \ell) + \min(|v_k|t, \ell) \left(\frac{1 - 2|a|^2}{\sqrt{(1 - 2|a|^2)^2 + 4|a|^4}} \right)^p \right], \quad (\text{A.28}) \end{aligned}$$

where in the first row we defined

$$b := \sum_{n=0}^{\infty} (-1)^n \widetilde{Z}_{2n} = \frac{1}{2(1 + (1 - 4|a|^2)^2)} - \frac{1}{4}, \quad (\text{A.29})$$

Here we should stress that Eq. (A.28) holds for even p , whereas for odd p one has that \widetilde{M}_p vanishes.

Appendix A.3. Fermionic negativity

We now have all the ingredients to compute the fermionic negativity. First, we notice that by using the results of section Appendix A.2, we can compute $\text{Tr}[\mathcal{F}(P^{-1}(\Gamma^+ + \Gamma^-))]$ for a generic function $\mathcal{F}(z)$ admitting a Taylor expansion around $z = 0$. After expanding $\mathcal{F}(z)$ around $z = 0$ and using (A.28) for each term in the expansion, we obtain that

$$\begin{aligned} \text{Tr}[\mathcal{F}(P^{-1}(\Gamma^+ + \Gamma^-))] &= \frac{1}{2} \int_{-k_F}^{k_F} \frac{dk}{2\pi} \left\{ \left(\frac{2\pi\ell}{k_F} - \min(|v_k|t, \ell) \right) (\mathcal{F}(1) + \mathcal{F}(-1)) \right. \\ &\quad \left. + \min(|v_k|t, \ell) \left[\mathcal{F}\left(\frac{1 - 2|a|^2}{\sqrt{(1 - 2|a|^2)^2 + 4|a|^4}} \right) + \mathcal{F}\left(-\frac{1 - 2|a|^2}{\sqrt{(1 - 2|a|^2)^2 + 4|a|^4}} \right) \right] \right\} \quad (\text{A.30}) \end{aligned}$$

The presence of the terms $\mathcal{F}(z) + \mathcal{F}(-z)$ follows from the fact that $\widetilde{M}_p = 0$ for odd p . Clearly, by choosing $\mathcal{F}(z) = z^p$, one recovers (A.28). To compute the negativity, we have to use the function (see the first term in (18))

$$\mathcal{F}(z) = \ln \left[\left(\frac{1+x}{2} \right)^{1/2} + \left(\frac{1-x}{2} \right)^{1/2} \right]. \quad (\text{A.31})$$

The second term in the definition of the negativity (see Eq. (18)) is obtained from the results of Ref. [24]. Putting everything together, we obtain that

$$\mathcal{E} = \frac{1}{2} \int_{-k_F}^{k_F} \frac{dk}{2\pi} \min(|v_k|t, \ell) \ln \left(2|a|^2 + \sqrt{(1 - 2|a|^2)^2 + 4|a|^4} \right). \quad (\text{A.32})$$

Similar to the von Neumann entropy [24], the negativity depends only on the absorption coefficient $|a(k)|^2$ of the lossy site.

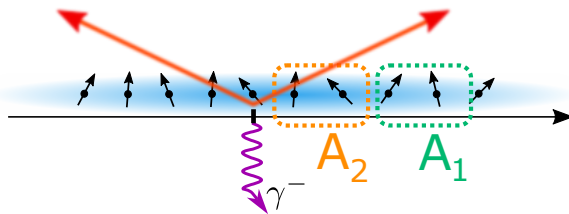


Figure B1. Two adjacent equal-length intervals A_1 and A_2 of size ℓ placed on the same side of the dissipative impurity. An entangled pair formed by the reflected and transmitted fermions scattered by the impurity is shown. As the two entangled particles are never shared between the two intervals the negativity between them is zero in the hydrodynamic limit.

Appendix B. The case of two unentangled intervals

In this section we consider the tripartition in Fig. B1. In contrast with Fig. 1 the two subsystems A_1 and A_2 are on the same side of the impurity. To be specific, let us take the two consecutive intervals $A_1 = [1, \ell]$ and $A_2 = [\ell + 1, 2\ell]$ as our subsystems. According to the scenario discussed in 4 (see also Fig. 1 (b)), the entanglement between two intervals is due to the pairs of entangled quasiparticles produced at the impurity, and shared between the intervals. As it is clear from Fig. B1 this implies that the two intervals A_1 and A_2 cannot be entangled because the pairs of quasiparticles produced at the impurity site are never shared between them.

It is instructive to prove this result using the approach of Appendix A. The fermionic correlation matrix G for $A_1 \cup A_2$ is given as

$$G = \begin{pmatrix} G^{11} & G^{12} \\ G^{21} & G^{22} \end{pmatrix} = \begin{pmatrix} G_{x,y} & G_{x,y+\ell} \\ G_{x+\ell,y} & G_{x+\ell,y+\ell} \end{pmatrix}, \quad x, y \in [1, \ell]. \quad (\text{B.1})$$

Notice that (B.1) is different from (A.1). As in the previous section, we can write

$$\Gamma_{x,y}^{\pm} := 2 \begin{pmatrix} G_{x,y} & \mp i G_{x,y+\ell} \\ \mp i G_{x+\ell,y} & -G_{x+\ell,y+\ell} \end{pmatrix} - \delta_{x,y} \sigma_z, \quad x, y \in [1, \ell]. \quad (\text{B.2})$$

We now proceed as in section Appendix A. We consider the moments

$$\widehat{M}_p(\{n_j\}) := \text{Tr} \left[\prod_{j=1}^p ((\Gamma^+ \Gamma^-)^{n_j} \Gamma^{\pm}) \right], \quad (\text{B.3})$$

and their truncated version \widehat{M}_p^t (cf. (A.7)), where the superscript t is to stress that we neglect the term σ_z in (B.2). Notice that, in contrast with the similar definition (A.7), here we do not sum over the \pm in Γ^{\pm} (notice the term $\Gamma^+ + \Gamma^-$ in (A.7)). Using the definition of $G_{x,y}$ in (A.1), we have

$$\Gamma_{x,y}^{\pm} = 2 \int_{-k_F}^{k_F} \frac{dk}{2\pi} S_{k,x}^{\pm} (S_{k,y}^{\pm})^{\dagger}, \quad (\text{B.4})$$

where we have defined $S_{k,x}^\pm$ as

$$S_{k,x}^\pm := \begin{pmatrix} S_{k,x} \\ \mp i S_{k,x+\ell} \end{pmatrix} = e^{ikx} \begin{pmatrix} 1 \\ \mp i e^{ik\ell} \end{pmatrix} + r(k) e^{i|k|x} \int_{-\infty}^{\infty} \frac{dq}{2\pi i} \frac{e^{i(|v_k|t-x)q}}{q - i0^+} \begin{pmatrix} 1 \\ \mp i e^{i(|k|-q)\ell} \end{pmatrix}, \quad (\text{B.5})$$

where $r(k)$ is the reflection coefficient (cf. (11)), and the integral over q yields the proper step functions (A.16). After substituting (B.4) and (B.5) in (B.3) for each couple of Γ s in (B.3) we have to evaluate sums of the type

$$\Sigma_1 := \sum_{x=1}^{\ell} (S_{k,x}^\pm)^\dagger S_{k',x}^\mp, \quad \Sigma_2 := \sum_{x=1}^{\ell} (S_{k,x}^\pm)^\dagger S_{k',x}^\pm. \quad (\text{B.6})$$

These sums can be rewritten by using the identity (A.12). We obtain terms of the type

$$F_{k_i,k_j}^{uu} = \frac{\ell}{4} \int_{-1}^1 d\xi w(k_i - k_j) e^{i\ell(\xi+1)(k_i-k_j)/2} (1 \pm e^{i\ell(k_i-k_j)}), \quad (\text{B.7})$$

$$F_{k_i,k_j}^{ud} = -\frac{\ell}{4} \int_{-1}^1 d\xi \int \frac{dq}{2\pi i} w(k_i - |k_j| + q) e^{i\ell(\xi+1)(k_i-|k_j|+q)/2} A_{k_j,q}^* (1 \pm e^{i\ell(k_i-|k_j|+q)}), \quad (\text{B.8})$$

$$F_{k_i,k_j}^{du} = \frac{\ell}{4} \int_{-1}^1 d\xi \int \frac{dq}{2\pi i} w(|k_i| - k_j - q) e^{i\ell(\xi+1)(|k_i|-k_j-q)/2} A_{k_i,q} (1 \pm e^{i\ell(|k_i|-k_j-q)}), \quad (\text{B.9})$$

and

$$F_{k_i,k_j}^{dd} = -\frac{\ell}{4} \int_{-1}^1 d\xi \int \frac{dq}{2\pi i} \int \frac{dq'}{2\pi i} w(|k_i| - |k_j| - q + q') e^{i\ell(\xi+1)(|k_i|-|k_j|-q+q')/2} A_{k_i,q} A_{k_j,q'}^* (1 \pm e^{i\ell(|k_i|-|k_j|-q+q')}), \quad (\text{B.10})$$

where $w(k) = k/\sin(k/2)$, and we defined $A_{k,q} := r(k) e^{i|v_k|q}/(q - i0^+)$ (the star denoting complex conjugation). The superscripts u and d , for example, in F_{k_i,k_j}^{ud} mean that in multiplying $(S^\alpha)^\dagger S^\beta$ (cf. (B.6)), with $\alpha, \beta = \pm$ we consider the first term in (B.5) for S^α and the second one for S^β . The u refers to the fact that the first term in (B.5) is present also in the unitary case, whereas d stands for ‘‘dissipative’’ because the second term in (B.5) is due to the dissipation.

The \pm signs in (B.7)(B.8)(B.9)(B.10) are fixed as follows: If we multiply S^+S^- or S^-S^+ they are all $+$, whereas if we multiply S^+S^+ or S^-S^- , we have all $-$ signs. The formulas (B.7)(B.8)(B.9)(B.10) can be simplified in the hydrodynamic limit $t, \ell \rightarrow \infty$ with their ratio t/ℓ fixed. In this limit the integrals in (B.7)-(B.10) are dominated by the points with $q, q' \rightarrow 0$ and $k_j \rightarrow \pm \bar{k}$ for all j . This means that we can replace $w(k) \rightarrow 2$ and perform the integration over q . We obtain

$$F_{k_i,k_j}^{uu} = \frac{\ell}{2} \int d\xi e^{i\ell(\xi+1)(k_i-k_j)/2} \pm e^{i\ell(\xi+3)(k_i-k_j)/2}, \quad (\text{B.11})$$

$$F_{k_i,k_j}^{ud} = \frac{\ell}{2} \int d\xi e^{i\ell(\xi+1)(k_i-|k_j|)/2} r(k_j) \Theta(-\ell(\xi+1)/2 + |v_{k_j}|t) \pm e^{i\ell(\xi+3)(k_i-|k_j|)/2} r(k_j) \Theta(-\ell(\xi+3)/2 + |v_{k_j}|t), \quad (\text{B.12})$$

$$F_{k_i, k_j}^{du} = \frac{\ell}{2} \int d\xi e^{i\ell(\xi+1)(|k_i|-k_j)/2} r(k_i) \Theta(-\ell(\xi+1)/2 + |v_{k_i}|t) \pm e^{i\ell(\xi+3)(|k_i|-k_j)/2} r(k_i) \Theta(-\ell(\xi+3)/2 + |v_{k_i}|t), \quad (\text{B.13})$$

and

$$F_{k_i, k_j}^{dd} = \frac{\ell}{2} \int d\xi e^{i\ell(\xi+1)(|k_i|-|k_j|)/2} r(k_i) r(k_j) \Theta(-\ell(\xi+1)/2 + |v_{k_i}|t) \Theta(-\ell(\xi+1)/2 + |v_{k_j}|t) \pm e^{i\ell(\xi+3)(|k_i|-|k_j|)/2} r(k_i) r(k_j) \Theta(-\ell(\xi+3)/2 + |v_{k_i}|t) \Theta(-\ell(\xi+3)/2 + |v_{k_j}|t). \quad (\text{B.14})$$

The two sums Σ_1 and Σ_2 (cf. (B.6)) contain a term of the form $\sum_{\alpha, \beta} F_{k_i, k_j}^{\alpha\beta}$.

To proceed, let us observe that in calculating the truncated moments \widehat{M}_p^t (cf. (B.3)), we have a multidimensional integral in the variables k_j and ξ_j with $j = 1, \dots, 2N_p + p$. We can now treat these integrals using the stationary phase approximation [70]. The integrand contains products of the form:

$$\prod_{i=1}^{2N_p+p} e^{i\ell\eta_i(k_{\sigma_i}-k_{\tau_{i-1}})/2} \tilde{r}^{\sigma_i}(\xi_i, k_{\sigma_i}) \tilde{r}^{\tau_{i-1}}(\xi_i, k_{\tau_{i-1}}), \quad (\text{B.15})$$

where η_i can be $\xi_i + 1$ or $\xi_i + 3$, k_{σ_i} , k_{τ_i} are defined in (A.14), \tilde{r}^{σ_i} are defined in (A.15), and $N_p := \sum_{j=1}^p n_j$. Now, it is easy to verify that the stationary point of (B.15) is in the integration domain *only* if all the η_i are the same. For instance, if we have $\eta_i = \xi_i + 1$ and $\eta_{i+1} = \xi_{i+1} + 3$, in (B.15) we have a term $((\xi_i + 1)k_{\sigma_i} + (\xi_{i+1} + 3)k_{\tau_i})/2$ in the exponent. Thus, the stationary point must satisfy the condition $\xi_i + 1 = \pm(\xi_{i+1} + 3)$, which has no solution because ξ_i are in $[-1, 1]$. This implies that

$$\widehat{M}_p^t = \ell^{2N_p+p} \int_{-k_F}^{k_F} \frac{d^{2N_p+p}k}{(2\pi)^{2N_p+p}} \int d^{2N_p+p}\xi \sum_{\sigma_i, \tau_i} \prod_{i=1}^{2N_p+p} e^{i\ell(\xi_i+1)(k_{\sigma_i}-k_{\tau_{i-1}})/2} \tilde{r}^{\sigma_i}(\xi_i, k_{\sigma_i}) \tilde{r}^{\tau_{i-1}}(\xi_i, k_{\tau_{i-1}}) + (-1)^p \left(\sum_{\sigma_i, \tau_i=0,1} \prod_{i=1}^{2N_p+p} e^{i\ell(\xi_i+3)(k_{\sigma_i}-k_{\tau_{i-1}})/2} \tilde{r}^{\sigma_i}(\xi_i, k_{\sigma_i}) \tilde{r}^{\tau_{i-1}}(\xi_i, k_{\tau_{i-1}}) \right). \quad (\text{B.16})$$

The variables $\sigma_i, \tau_i = 0, 1$ have the same meaning as in (A.13). The first term in (B.16) corresponds to the choice $\eta_i = \xi_i + 1$ for any i , and the second one is for $\eta_i = \xi_i + 3$ (cf. (B.15)). Now, the first term in (B.16) is the same as in Ref. [24]. The second one has the same structure, the only difference being that one has to replace $\xi_i \rightarrow \xi_i + 2$. Following Ref. [24], we obtain

$$\widehat{M}_p^t = 2^{2N_p+p} \int_{-k_F}^{k_F} \frac{dk}{2\pi} \left[\ell - \frac{1}{2} \min(|v_k|t, \ell) + \frac{1}{2} (1 - |a(k)|^2)^{2N_p+p} \min(|v_k|t, \ell) \right] + (-1)^p \left[\ell - \frac{1}{2} \max(0, \min(|v_k|t - \ell, \ell)) + \frac{1}{2} (1 - |a(k)|^2)^{2N_p+p} \max(0, \min(|v_k|t - \ell, \ell)) \right] \quad (\text{B.17})$$

where to derive the second term we used that

$$\int_{-1}^1 d\xi \Theta(-\ell(\xi+3)/2 + t|v_k|) = 2 \max(0, \min(|v_k|t/\ell - 1, 1)). \quad (\text{B.18})$$

Let us now consider the effect of the term $\delta_{x,y}\sigma_z$ (cf. (B.2)). The idea is that one can replace any occurrence of a G matrix in the definitions of Γ^\pm with $\delta_{x,y}\sigma_z$. The result is

$$\begin{aligned} \widehat{M}_p(\{n_j\}) &= \sum_{i=0}^p \binom{p}{i} 2^{p-i} (-1)^i \sum_{j_1=0}^{2n_1} \binom{2n_1}{j_1} 2^{2n_1-j_1} (-1)^{j_1} \dots \sum_{j_p=0}^{2n_p} \binom{2n_p}{j_p} 2^{2n_p-j_p} (-1)^{j_p} \\ &\quad \int_{-k_F}^{k_F} \frac{dk}{2\pi} \left[\ell - \frac{1}{2} \min(|v_k|t, \ell) + \frac{1}{2} (1 - |a(k)|^2)^{p-i+\sum_{l=1}^p (2n_l-j_l)} \min(|v_k|t, \ell) \right] \\ &+ (-1)^p \left[\ell - \frac{1}{2} \max(0, \min(|v_k|t-\ell, \ell)) + \frac{1}{2} (1 - |a(k)|^2)^{p-i+\sum_{l=1}^p (2n_l-j_l)} \max(0, \min(|v_k|t-\ell, \ell)) \right]. \end{aligned} \quad (\text{B.19})$$

The sums and the combinatorial factors in the first row in (B.19) account for all the possible insertions of $\delta_{x,y}\sigma_z$. By comparing (B.17) with (B.19) it is clear that the effect of replacing the G matrix with the term $\delta_{x,y}\sigma_z$ is an overall minus sign, a factor 1/2 for each insertion, and a lowering of the exponent of the terms $(1 - |a(k)|^2)$. Notice that the case in which we replace all the Γ^\pm s with $\delta_{x,y}\sigma_z$ has to be treated separately, as we will discuss in the following. The sums in (B.19) can be performed exactly, yielding

$$\begin{aligned} \widehat{M}_p &= \int_{-k_F}^{k_F} \frac{dk}{2\pi} \left[\frac{\pi}{k_F} \ell - \frac{1}{2} \min(|v_k|t, \ell) + \frac{1}{2} (1 - 2|a(k)|^2)^{p+N_p} \min(|v_k|t, \ell) \right] + \\ &+ (-1)^p \left[\frac{\pi}{k_F} \ell - \frac{1}{2} \max(0, \min(|v_k|t - \ell, \ell)) + \frac{1}{2} (1 - |a(k)|^2)^{p+N_p} \max(0, \min(|v_k|t - \ell, \ell)) \right]. \end{aligned} \quad (\text{B.20})$$

The term $\pi/k_F \ell$ in the square brackets in (B.20) corresponds to replacing all the Γ^\pm with $\delta_{x,y}\sigma_z$.

To compute the negativity (cf. (18)), we have to evaluate traces of powers of $P^{-1}(\Gamma^+ + \Gamma^-)$, where $P = \mathbb{1} + \Gamma^+\Gamma^-$. We proceed as in Appendix A, rewriting P^{-1} as

$$P^{-1} = \sum_{n=0}^{\infty} (-1)^n (\Gamma^+\Gamma^-)^n. \quad (\text{B.21})$$

After using (B.20), and after summing over the variables $n_j \in [0, \infty)$ in (B.20), we obtain

$$\begin{aligned} \text{Tr} \left[(P^{-1}(\Gamma^+ + \Gamma^-))^p \right] &= \\ &\quad \int_{-k_F}^{k_F} \frac{dk}{2\pi} \left[\frac{\pi}{k_F} \ell - \frac{1}{2} \min(|v_k|t, \ell) + \frac{1}{2} \left(\frac{2(1 - 2|a(k)|^2)}{1 + (1 - 2|a(k)|^2)^2} \right)^p \min(|v_k|t, \ell) \right] \\ &+ (-1)^p \left[\frac{\pi}{k_F} \ell - \frac{1}{2} \max(0, \min(|v_k|t - \ell, \ell)) + \frac{1}{2} \left(\frac{2(1 - 2|a(k)|^2)}{1 + (1 - 2|a(k)|^2)^2} \right)^p \max(0, \min(|v_k|t - \ell, \ell)) \right], \end{aligned} \quad (\text{B.22})$$

where we have used the regularisation $\sum_{n=0}^{\infty} (-1)^n = 1/2$. It is straightforward to extend the result (B.22) to the trace of arbitrary functions of $P^{-1}(\Gamma^+ + \Gamma^-)$. For an analytic

function \mathcal{F} , one finally obtains:

$$\begin{aligned} \text{Tr} [\mathcal{F}(P^{-1}(\Gamma^+ + \Gamma^-))] = & \\ & \int_{-k_F}^{k_F} \frac{dk}{2\pi} \left[\mathcal{F}(1) \left(\frac{\pi}{k_F} \ell - \frac{1}{2} \min(|v_k|t, \ell) \right) + \frac{1}{2} \mathcal{F} \left(\frac{2(1 - 2|a(k)|^2)}{1 + (1 - 2|a(k)|^2)^2} \right) \min(|v_k|t, \ell) \right. \\ & \left. + \mathcal{F}(-1) \left(\frac{\pi}{k_F} \ell - \frac{1}{2} \max(0, \min(|v_k|t - \ell, \ell)) \right) + \frac{1}{2} \mathcal{F} \left(-\frac{2(1 - 2|a(k)|^2)}{1 + (1 - 2|a(k)|^2)^2} \right) \max(0, \min(|v_k|t - \ell, \ell)) \right]. \end{aligned} \quad (\text{B.23})$$

As it is clear from (18), to evaluate the negativity, we have to use the function

$$\mathcal{F}(x) = \ln \left(\sqrt{\frac{1+x}{2}} + \sqrt{\frac{1-x}{2}} \right), \quad (\text{B.24})$$

which is even and for which $\mathcal{F}(\pm 1) = 0$. We obtain the quite simple formula

$$\text{Tr} [\mathcal{F}(P^{-1}(\Gamma^+ + \Gamma^-))] = \int_{-k_F}^{k_F} \frac{dk}{2\pi} \mathcal{F} \left(\frac{2(1 - 2|a(k)|^2)}{1 + (1 - 2|a(k)|^2)^2} \right) \min(|v_k|t/2, \ell). \quad (\text{B.25})$$

To obtain the negativity, we need the second term in (18). This is obtained from the results of Ref. [24] as

$$\text{Tr} [\tilde{\mathcal{F}}(G)] = \int_{-k_F}^{k_F} \frac{dk}{2\pi} \tilde{\mathcal{F}}(1 - |a(k)|^2) \min(|v_k|t/2, \ell), \quad (\text{B.26})$$

with

$$\tilde{\mathcal{F}}(x) := \ln(\sqrt{x^2 + (1-x)^2}). \quad (\text{B.27})$$

In (B.26) G is the correlation matrix (6) restricted to $A_1 \cup A_2$. It is straightforward to show that the sum of (B.25) and (B.26) vanishes.

Appendix C. Single fermion with a localized loss

Here we study the dynamics of a single fermion with momentum k in the presence of a localized fermionic loss (see Ref. [32] for a similar setup). The system is a chain of L sites. We work on a finite lattice, to have normalized states in what follows. The generic initial condition for a single fermion in a pure state $\rho(0)$ is:

$$\rho(0) = \sum_{n,m} \psi_n(0) c_n^\dagger |0\rangle \langle 0| c_m \psi_m^*(0). \quad (\text{C.1})$$

Here c_n^\dagger are fermionic creation operators, $|0\rangle$ is the fermion vacuum, and $\psi_n(0)$ the wavefunction amplitudes. The time evolution (5) will transform the state into a mixed state $\rho(t)$ as

$$\rho(t) = \sum_{n,m} \psi_n(t) c_n^\dagger |0\rangle \langle 0| c_m \psi_m^*(t) + C(t) |0\rangle \langle 0|, \quad (\text{C.2})$$

where $C(t)$ is a parameter representing the probability of having lost the fermion at time t . The amplitudes $\psi_n(t)$ satisfy the system of equations

$$\frac{d\psi_n}{dt} = i(\psi_{n+1} + \psi_{n-1}) - \frac{\gamma}{2}\delta_{n,0}\psi_0. \quad (\text{C.3})$$

If we start from a plane wave $\psi_n(0) = L^{-1/2}e^{ikn}$, in the hydrodynamic limit $n, t \rightarrow \infty$ the solution of (C.3) is (see [29])

$$\psi_n(t) = \frac{1}{\sqrt{L}}e^{-i\varepsilon_k t}(e^{ikn} + r(k)\Theta(|v_k|t - |n|)e^{i|kn|}), \quad (\text{C.4})$$

where ε_k is the same energy dispersion in (4) and v_k is the fermion velocity. In the following, we consider as initial condition for our fermion the symmetric wavefunction $\psi_n(0) = (e^{ikn} + e^{-ikn})/\sqrt{2}$; by exploiting the linearity of (C.3), it is immediate to obtain from (C.4) the expression for $\psi_n(t)$.

Let us now compute the fermionic negativity between two intervals of equal length ℓ , $A = [-\ell, -1]$ and $B = [1, \ell]$. The reduced density matrix of the two subsystems is obtained, by tracing over the rest of the chain, as

$$\rho_{AB}(t) = \sum_{|n|, |m|=1}^{\ell} \psi_n(t)c_n^\dagger|0\rangle\langle 0|c_m\psi_m^*(t) + M(t)|0\rangle\langle 0| := |\psi(t)\rangle\langle\psi(t)| + M(t)|0\rangle\langle 0|, \quad (\text{C.5})$$

where now $|0\rangle$ is the vacuum of fermions in region $A \cup B$ and $M(t)$ the probability for the fermion being absorbed or being outside region A . The state $|\psi(t)\rangle$ is clearly non-normalized. It is convenient to rewrite the previous equation as:

$$\rho_{AB}(t) = |\psi(t)|^2 |\psi_N(t)\rangle\langle\psi_N(t)| + M(t)|0\rangle\langle 0|, \quad (\text{C.6})$$

where the subscript N means "normalized", and we have $\text{Tr}[\rho_{AB}] = |\psi|^2 + M = 1$. For our initial condition, we have:

$$|\psi|^2 := p^2 = \sum_{|n|=1}^{\ell} \psi_n^*(t)\psi_n(t) = \frac{2\ell}{L} \left(1 - |a(k)|^2 \min\left(\frac{|v_k|t}{\ell}, 1\right) \right) + O\left(\frac{1}{L}\right). \quad (\text{C.7})$$

To construct the partial transpose, we rewrite the density matrix in a basis that is a tensor product of a basis of A and one of B . We define:

$$|\psi_A(t)\rangle = \sum_{n=-\ell}^{-1} \psi_n(t)c_n^\dagger|0\rangle = \frac{p}{\sqrt{2}}|\psi_{A,N}(t)\rangle; \quad (\text{C.8})$$

$$|\psi_B(t)\rangle = \sum_{n=1}^{\ell} \psi_n(t)c_n^\dagger|0\rangle = \frac{p}{\sqrt{2}}|\psi_{B,N}(t)\rangle. \quad (\text{C.9})$$

Since $|\psi\rangle = |\psi_A\rangle + |\psi_B\rangle$, we can rewrite the density matrix in the basis $\{|0_A\rangle, |\psi_{A,N}\rangle\} \otimes \{|0_B\rangle, |\psi_{B,N}\rangle\}$ as:

$$\rho_{AB}(t) = \begin{pmatrix} M & 0 & 0 & 0 \\ 0 & p^2/2 & p^2/2 & 0 \\ 0 & p^2/2 & p^2/2 & 0 \\ 0 & 0 & 0 & 0 \end{pmatrix} \quad (\text{C.10})$$

And the partial transpose with respect to one of the two subsystems reads:

$$\rho_{AB}^{\text{T}_B}(t) = \begin{pmatrix} M & 0 & 0 & p^2/2 \\ 0 & p^2/2 & 0 & 0 \\ 0 & 0 & p^2/2 & 0 \\ p^2/2 & 0 & 0 & 0 \end{pmatrix}, \quad (\text{C.11})$$

with eigenvalues $\{p^2/2, p^2/2, (M + \sqrt{M^2 + p^4})/2, (M - \sqrt{M^2 + p^4})/2\}$. The negativity is, then:

$$\mathcal{E} = \text{Tr}(\ln |\rho_{AB}^{\text{T}_B}|) = \ln \left(1 - M + \sqrt{M^2 + (1 - M)^2} \right) \quad (\text{C.12})$$

Formula (C.12) describes how the initial negativity $\mathcal{O}(\ell/L)$ decreases with time. Notice that (C.12) becomes the negativity content in (23) after defining $1 - M \rightarrow 2|a(k)|^2$.

The single-fermion negativity sheds some light on the many-fermion case treated in the main text. Let us start from the state $b_k^\dagger b_{-k}^\dagger$. This state can be considered as a toy version of the Fermi sea. Also, the state b_k^\dagger and b_{-k}^\dagger can be interpreted as the transmitted and reflected fermions, respectively. One can rewrite $b_k^\dagger b_{-k}^\dagger$ as

$$b_k^\dagger b_{-k}^\dagger = \left(\frac{b_k^\dagger + b_{-k}^\dagger}{\sqrt{2}} \right) \left(\frac{b_k^\dagger - b_{-k}^\dagger}{\sqrt{2}} \right). \quad (\text{C.13})$$

Now, it is easy to show that the antisymmetric combination $b_k^\dagger - b_{-k}^\dagger$ anticommutes with the Lindblad operator $\sqrt{\gamma^-}c_0$, and does not evolve with time. On the other hand, the fermion in the symmetric combination can be absorbed at the impurity. After the fermion is absorbed, only the entangled antisymmetric combination remains.